DETERMINATION OF PULSATION PERIODS OF DELTA SCUTI VARIABLE STARS USING UBVRI PHOTOMETRY

By

G.R.D.S. Godagama
(S/10/719)

Supervised by

Dr. T. P. Ranawaka
(Department of physics, University of Peradeniya)

Mr. S. Gunasakara and Mr. J. Adasuriya
(Space Application Division of Arthur C. Clark Institute of Modern Technologies, Moratuwa)

Department of physics, Faculty pf science, University of Peradeniya-2015

DETERMINATION OF PULSATION PERIODS OF DELTA SCUTI VARIABLE STARS USING UBVRI PHOTOMETRY

A PROJECT REPORT PRESENTED BY

G.R.D.S. GODAGAMA

In partial fulfilment of the requirement

For the award of the degree of

B.Sc. (physics special)

Of the

Faculty of Science,

University of Peradeniya,

Sri Lanka.

2014/2015

ACKNOWLEDGEMENT

ABSTRACT

DETERMINATION OF PULSATION PERIODS OF DELTA SCUTI VARIABLE STARS USING UBVRI PHOTOMETRY

The purpose of this research was to do a photometric study on Delta Scuti variable stars, SZ Lyn, YZ Boo and ZZ Mic. Also, to determine the pulsation periods of these variable stars. CCD observational data were obtained using the 45cm cassegrain telescope at Arthur C. Clark Institute of modern technologies, Srilanka and a 14" Newtonian reflection telescope along with an Apogee Alta F9000 CCD Camera and an Apogee FW509R filter wheel. SZ Lyn was observed using Johnson B,V and R filters. YZ Boo and ZZ Mic were observed using only Johnson V filter. Images were reduced and digital photometry were carried out using Image Reduction and Analysis Facility (IRAF). Light curves of variable stars were obtained using the differential photometry method and the frequency analysis was done using both least square spectral analysis (Lomb-Scragle method) and discrete Fourier transformation. VARTOOLS light curve analysis program was used in frequency analysis.

Three pulsation periods were detected in SZ Lyn. Fundamental vibration and the first overtone of radial vibrations in SZ Lyn were identified by examining period ratios. Main pulsation periods of YZ Boo and ZZ Mic were measured. Average densities of observed variable stars were calculated using Eddington's period density relationship.

LIST OF FIGURES

LIST OF TABLES

TABLE OF CONTENTS

CHAPTER 01

INTRODUCTION

1.1 Introduction to variable stars

1.1.1 Variability of stars

A star which changes its brightness with the time, as seen by an external observer, is known as a variable star. In most of the cases, these changes are periodic and can have periods from a fraction of second to years. Brightness fluctuation can range from 0.001 to 20 magnitudes. The oldest preserved historical document of a variable star has been created 3200 years ago by the ancient Egyptians [1]. The first modern identified variable star was Omicron Ceti, later renamed Mira. It had been described as a nova in 1596 by David Fabricius. In 1638, Johannes Holwards observed Omicron Ceti pulsating in a regular 11-month cycle [2]. This was an important discovery, as it helped to verify that the stars were not eternal and invariable as ancient philosophers like Aristotle and Ptolemy had believed. The discovery of variable stars paved the way for development of the science of astronomy. Today, over 100000 variable stars are known and have been catalogued. About a same number of stars are suspected to be variable. [3]

Variability can be caused by a luminosity change in the star or a change in the amount of light which can reach the observer. Variable stars are divided into two main categories depending on the above principle. Stars which exhibit variability due to a luminosity change are known as intrinsic variables. Stars which show variability only due to a change in the amount of light which can reach the observer are known as extrinsic variables. Also, variable stars are divided into several sub categories depending on the spectral class, period and mechanisms which cause the variability.
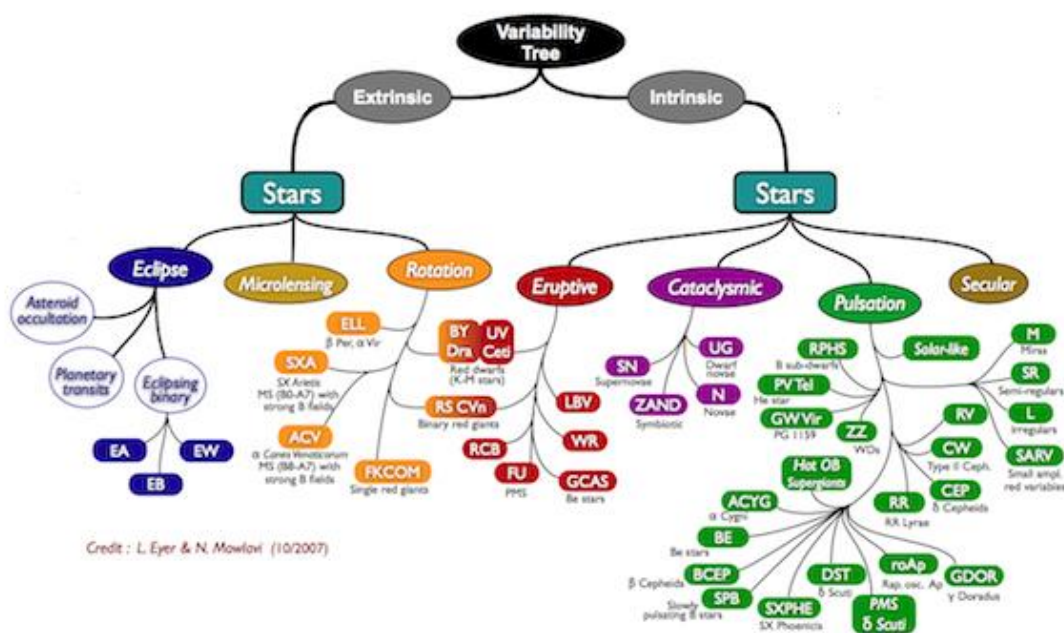
Figure 1.01 categories of variable stars [4]

1.1.2 Pulsating variable stars

Pulsating variable stars exhibit their variability due to periodic shrinks and swells of the stellar outer layers so that the star is observed to be pulsating. Since these pulsations affect the stellar luminosity, pulsating variable stars are categorized as intrinsic variables. These pulsation occur due to an unbalance between the inward gravitational force and the outward radiation pressure. In a normal stable star, gravitational attraction and the radiation pressure are balanced and the star is said to be in a hydrostatic equilibrium. But if the gravity is dominating over the radiation pressure, star starts to shrink and vice versa.

Pulsations can be radial or non-radial. In radial pulsations, star expands and shrinks as a whole. Non-radial pulsations occur in the stars surface. Hence they can be described using spherical harmonics. There is a natural fundamental frequency which determines the period of a pulsating star. But stars may also pulsate in a harmonic or overtone which is a higher frequency, corresponding to a shorter period. Often, they pulsate simultaneously with multiple frequencies. Therefore, a complex analysis is required to determine the separate interfering periods. Studying those pulsations help to reveal information about the stellar structure and composition. The study of stellar interiors using their pulsations is asteroseismology. [5]
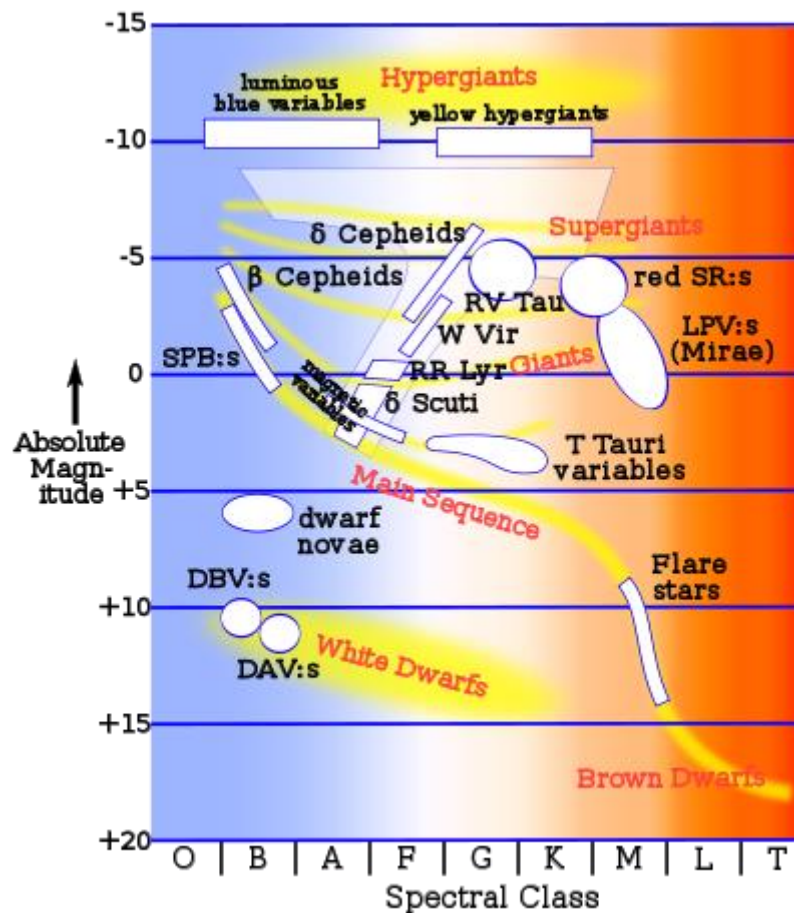
Figure 1.02 Variables star classification in the HR Diagram [5]

Pulsating stars are not generally found on the main sequence. Instead, most pulsating stars occupy a narrow, vertical band on the right hand side of the HR diagram. This is called the instability strip

1.1.3 Delta Scuti variable stars

Delta Scuti variable stars are short period pulsating variable stars. Their main pulsation periods are less than 0.5 days. These stars generally belong to the spectral type A0 to F5, giants or main sequence stars. They exhibit luminosity variations due to both radial and non-radial pulsations. Typical brightness fluctuations are from 0.003 to 0.9 magnitudes. These type of pulsation variables were first found in 1900 by William W. Campbell and William H. Wright. [6] It was a giant star in the southern constellation Scutum, called δ Scuti. The group of this pulsation stars were named after the prototype star. Delta Scuti variables have a He

Figure 1.03 Light Curve of well-known Delta Scuti star HT 515 [7]

rich atmosphere. Ionized He in outer layers tend to scatter radiation partially blocking the radiation from going out of the star. As a result, radiation pressure increases and starts to push outer layers against the gravity and the star expands. After expanding several kilometers from the center, outer layers cool down and ionized He convert to atomic He allowing the radiation to pass through. Then radiation pressure decreases again and gravity become dominant over radiation pressure, causing the star to shrink towards the center. This continues as a cyclic process allowing the star to pulsate. Delta Scuti variables are also known as Dwarf Cepheid because of their similar properties to Cepheid variables. Both Cepheid and Delta Scuti variables have a well-defined Period-Luminosity relationship which has been used to establish the distances to the galaxies.

The most up-to-date catalogue of Delta Scuti stars was provided by Rodr´ıguez et al. (2000). It contains a summary of all the observational characteristics of more than 600 Delta Scuti stars that had been studied up until 2000. [8] A comprehensive analysis of the properties of all these stars was made by Rodr´ıguez & Breger (2001). Montgomery & Breger (2000) and Zverko et al. (2004) present the proceedings of two international meetings on, respectively, Delta Scuti variables and related stars, and A stars in general, containing a wealth of information. A few Delta Scuti stars have been observed from space. For exasmple, θ² Tau and Altair with the star tracker on the WIRE (Wide-field InfraRed Explorer) satellite (Poretti et al. 2002; Buzasi et al. 2005, respectively), and HD263551 with the MOST (Microvariablity and Oscillations of STars) satellite. [9]

In this research, a photometric study was done on three Delta Scuti variable stars. SZ Lyn was selected as the primary target star. Photometric analysis was mainly done on SZ Lyn to identify the main pulsation period as well as its harmonics. Images were obtained with high time resolution for SZ Lyn. Other two stars, YZ Boo and ZZ Mic images were obtained with a lower time resolution and therefore, only the main pulsation periods were calculated.

Table 1.1

Observational data of target objects [10]

Star	Coordinates		Average magnitude	constellation
	RA	DEC		
SZ Lyn	$08^h\ 09^m\ 35.75^s$	$+44^0\ 28'\ 17.61''$	+9.08	Lynx
YZ Boo	$15^h\ 24^m\ 07.00^s$	$+36^0\ 52'\ 00.60''$	+10.36	Boots
ZZ Mic	$21^h\ 00^m\ 35.20^s$	$-42^0\ 39'\ 20.30''$	+9.43	Microscopium

1.1.4 Period density relation of variable stars

Eddington (1914) proposed that pulsating stars can be considered as thermodynamic heat engines, which radial oscillations may be the result of sound waves resonating in the stellar interior. [11] And the pulsations are similar to the vibrations in a stressed rope or an organ pipe.

The pulsation frequencies are eigenfrequencies of the star. They are similar to the eigenfrequencies of a stressed rope. Pressure and gravitation act as restoring forces in a star similar to stresses in a rope. Waves are converged and reflected at the center of the star which is constrained to vibrate so the center act as a node (Like ends of a stressed rope). At the surface of the star vibration amplitudes can be very large so the surface act as an anti-node. Pressure forces determine the phase velocity of the standing wave and therefore the sound velocity. By taking these pulsation periods into account, the average density and internal structure of the star can be estimated.
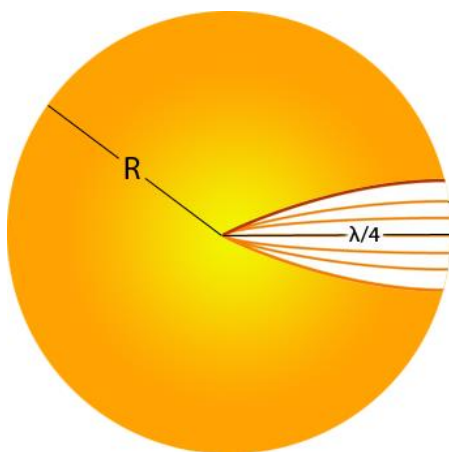
Figure 2.04 Fundamental radial vibration in a star
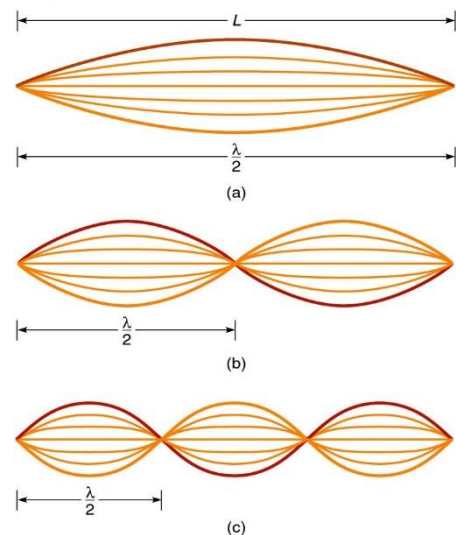
Figure 3.05 Vibrations on a stressed rope

Therefore, by considering the fundamental vibration, the pulsation period can be expressed as follows.

$$P \approx \frac{4R}{v} \qquad (1.01)$$

Where,

       P   -*Main pulsation period*

       R   -*Radius of star*

       v   -*Average sound velocity*

Velocity of sound in a gas medium can be expressed as,

$$\nu \approx \sqrt{\frac{\gamma.P_{gas}}{\rho_{avg}}} \qquad (1.02)$$

Where, γ is the ratio of specific heat capacities.

Simplest stellar structure models assume that stars are at a spherically symmetric hydrostatic equilibrium at their steady state, an equilibrium governed by inward gravitational forces and outward pressure gradient forces. Hydrostatic equation for stars can be expressed as follows.
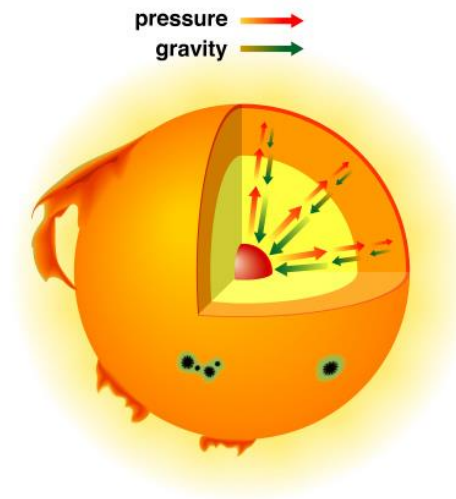
Figure 4.06 Hydrostatic equilibrium of a star, governed by inward gravitation and outward pressure

$$\frac{P_{gas}}{\rho_{avg}} \approx \frac{GM}{R} \qquad (1.03)$$

Where,

   P_{gas} -Gas pressure
   ρ_{avg} -Average density of star
   M -Mass of star
   G -Universal gravitational constant

Assuming the star as a uniform sphere, average density can be expressed as follows.

$$\rho_{avg} \approx \frac{3M}{4\pi R^3} \qquad (1.04)$$

From above equations, relationship between the average density and the pulsation period can be expressed as follows,

$$\rho_{avg} \approx \frac{12}{\pi G\gamma P^2} \qquad (1.05)$$

But in stars, temperature and density increase by orders of magnitudes from the outside towards the inside, therefore, slightly different from a rope. For more realistic stellar models, which are polytropes for $P \propto \rho^{(n+1/n)}$ for different n, different degrees of mass concentration towards the center are found (For n=3, as for the γ=5/3 for monoatomic gas).

Ratios of the eigenfrequencies depend on the density stratifications in the stars, therefore different from those of the rope. Using computational models it has been found that the ratio between fundamental period (P_0) and the period of 1st overtone (P_1), P_1/P_0=0.281 and P_1/P_2=0.639 for homogenous stars, while for the more realistic polytrope with n=3, P_1/P_0=0.687 and P_1/P_2=0.749. The ratio P_1/P_2 increased by more than a factor of 2 compared to the homogenous density model. Therefore, by obtaining period ratios, important conclusions about the density profile of the star can be made.

Different stellar models give different period ratios values. Also, it depends on the stellar mass. Henyey method is the most used stellar model for calculated density profile. The above period ratio values were calculated from the Henyey method. [12]

1.2 Introduction to Photometry

1.2.1 Photometry

Photometry is the science of the measurement of light, in terms of its perceived brightness to the human eye. Most of the astronomical studies involve measuring flux from a celestial object. Since variable stars change its brightness over time, the study of variable stars directly involves photometry. Generally, photometry is carried out by gathering light from a celestial object using a telescope and passing it through optical filters and then measuring the flux using photosensitive devices like CCDs.

In astronomy, a magnitude scale has been introduced to represent the flux from terrestrial objects. This magnitude scale was first invented by a Greek astronomer named Hipparchus.[13] He classified stars into 6 magnitude groups, decreasing the brightness from 1 to 6. The magnitude scale which been used today, is a modified version of the Hipparchus system.

According to the new magnitude scale, apparent magnitude of a celestial object is given by the following equation.

$$m = -2.5 \log(flux) + C \tag{1.06}$$

Where,

    m   - Apparent magnitude of the celestial object
    flux   - Measured flux from the object
    C   - Zero point constant

Zero point constant can be calculated using the flux from the reference star. Usually Vega is selected as the reference star.

1.2.2 Digital Photometry

In early days, photometry was carried out using photomultiplier tubes and photo electric photometers. Tha main drawback of these equipment was they can measure the light from only one object at a time. But nowadays, with the development of electronics, they have been replaced by Charge Couple Devices which are more reliable, fast and capable of simultaneously imaging multiple objects. CCDs are semiconductor chips which can act like an array of photometers. Using advanced electronics, flux values measured by every point (pixel) of the array, can be recorded into a digital image. These obtained images can be analyzed using computer software to calculate the magnitudes of observed objects.

1.2.3 Differential Photometry

Differential photometry is the most convenient and reliable photometric method used in variable star astronomy. In this method, both target and comparison objects are observed using the same photometric device and filters through the same optical path at the same time. Most of the observational variables which need calibrations, can be dropped out by simply considering the magnitude difference between the target object and the comparison object.

Differential photometry can be used to eliminate the atmospheric extinction from magnitude. When the light travels thought the atmosphere, part of it will not reach the telescope due to scattering and absorption by the atmosphere. This lost amount depends on the path length which light travels though the atmosphere (airmass). This path length changes as the object moves across the sky. Therefore atmospheric extinction is changing. Atmospheric extinction can be easily eliminated using differential photometry method.

To eliminate atmospheric extinction, a star field which contains the variable star as well as two nearby non-variable stars (named as comparison star and check star) was imaged. Since the path length is the same for these three stars, atmospheric extinction is the same. By considering the differential magnitude of variable star and the check star, atmospheric extinction can be eliminated. Another non variable star (Check Star) can be used to confirm the non-variability of the comparison star.
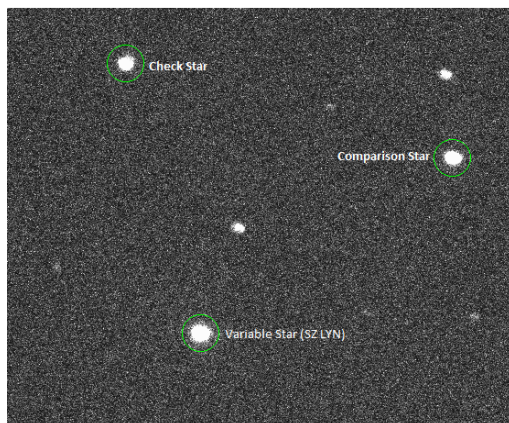
Figure 1.07 Selected star field contains variable star comparison star and check star
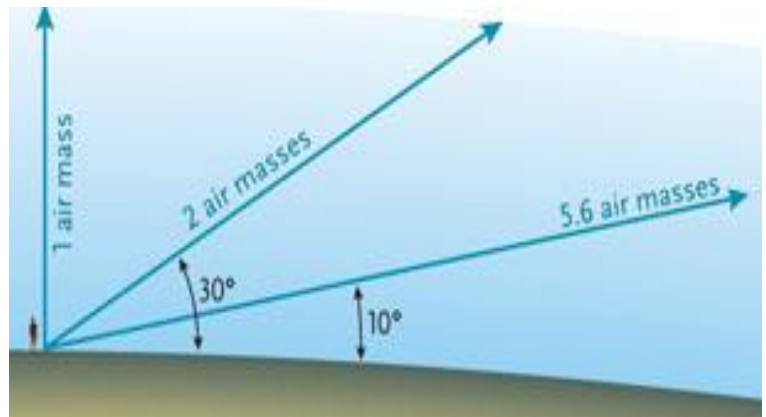
Figure 1.08 Variation of airmass as the star field move across the sky

$$Diff.Mag = Mag._{variable\ star} - Mag._{Comparison\ star} \quad (1.07)$$

$$Diff.Mag_{CC} = Mag._{Comparison\ star} - Mag._{Check\ star} \quad (1.08)$$

Diff. Mag is independent of the atmospheric extinction. Also. Diff. Mag$_{CC}$ can be used to check the non-variability of comparison star. If both check star and comparison star are non-variable, Diff. Mag$_{CC}$ must be constant with time.

1.2.4 Blackbody radiation from stars

In astronomy, photometry is simply the measuring of flux from stars. Radiation of energy from stars in the form of electromagnetic radiation can be described using blackbody radiation. Perfect blackbodies are capable of emitting and absorbing all kinds of electromagnetic radiation. Even though the stars are practically not perfect blackbodies since stellar atmosphere absorbs radiation belongs to some wavelengths, for most of the cases it will do no harm considering stars as perfect blackbodies.

Blackbodies exhibit a characteristic radiation curve as known as blackbody curve, which is shown in the figure 1.9. In 1893, Wilhelm Wien discovered an important relationship between the surface temperature of a blackbody and the wavelength of peak emission which is now called as Wien's displacement law.[14] He found that the shape of the blackbody curve would shift proportionally in wavelength with the temperature. The relationship can be mathematically expressed as follows.
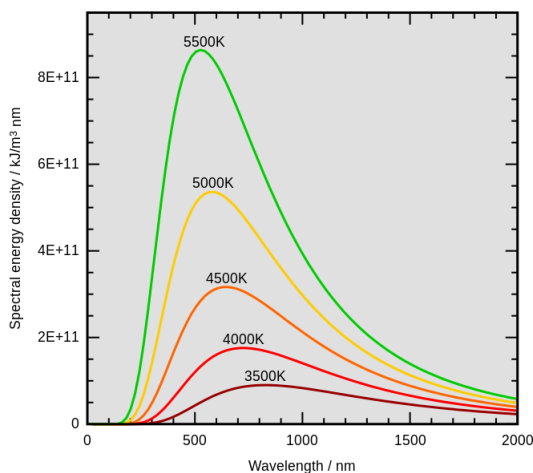
Figure 1.09 Characteristic radiation curve of a blackbody [15]
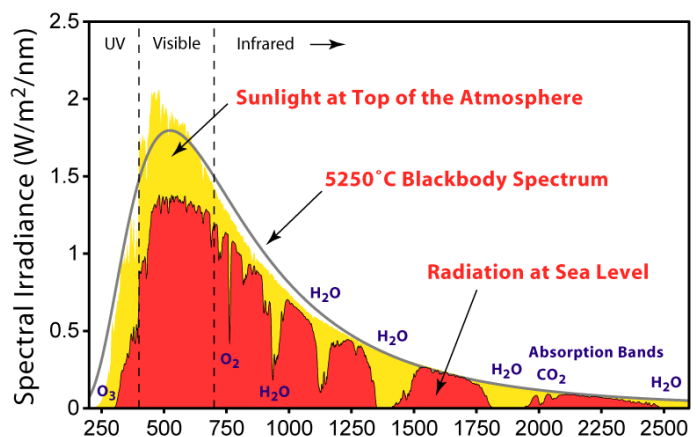
Figure 1.10 Radiation curve of the sun, practically different from a perfect blackbody [16]

$$\lambda_{max} = \frac{0.002897755\ mK}{T} \tag{1.09}$$

Where,
λ_{max} - Wave length of peak emission
T - Surface temperature of the blackbody

Consequently, this explains that blackbodies (in this case stars) which have higher surface temperature appear in blue color and stars which have lower surface temperature appear in red color. Table 2 contains visual colors and surface temperature of some prominent stars.

1.2.5 Color index

Color index is a numerical measure of the color of a blackbody. By examining the color index conclusions about the surface temperature of stars can be made. In astronomy, commonly used color indices are known as B-V, V-R, U-B and R-I which are derived from the Johnson UBVRI filter system (Filter systems will be disused in the chapter-03). Each letter (U,B,V,R,I) corresponds to a certain band of wavelength(a filter) and B-V is the difference of the measured magnitude when the star is observed through the B filter and V filter. Therefore, to measure the color index, magnitude of object must be measured successively through two different filters.

In this study, only three filters (B,V and R) were used and therefore B-V and V-R color indexes can be calculated. The smaller the color index, the bluer (or hotter) the object is. Conversely, the larger the color index, the more red (or cooler) the object is.

Table 1.2

Colors and surface temperatures of prominent stars [17]

Star	color	B-V	Surface Temperature (K)
Bellatrix	Blue	-0.21	28000
Sirius	Blue	-0.03	25200
Vega	White	0.00	9600
Sun	yellow	+0.65	5800
Betelgeuse	red	+1.85	2900

F. J. Ballesteros has introduced an approximate formula to calculate the surface temperature of a star directly from the B-V color index. It is known as Ballesteros' formula.[17] Formula is given as follows.

$$T = 4600 \left\{ \frac{1}{0.92(B-V)+1.7} + \frac{1}{0.92(B-V)+0.62} \right\} \qquad (1.10)$$
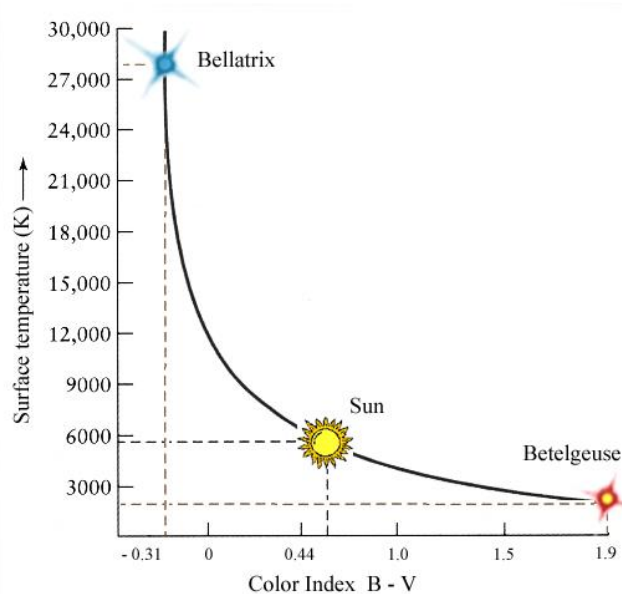
Figure 1.11 The curve surface temperature vs. color index of stars [17]

1.3 Introduction to astronomical time-series analysis

1.3.1 Light curves of variable stars

Light curve of a variable star is the plot of magnitude vs. time. Differential magnitude can be used for convenience. Usually Julian date is used as the time unit in the light curves. Julian day number is the continuous count of days since the beginning of the Julian period which is starting at noon on 1st January, 4713 BC. Julian dates are expressed as a Julian day number with a decimal fraction added. Decimal fraction represents how many hours, minuets or seconds have lapsed since the last Julian date. For example, the Julian Date for 00:30:00.0 UT January 1, 2013, is 2456293.520833 . [18]

Light curve is characteristic and holds important information about the stellar interior structure, composition and its seismology. Those information can be extracted using a proper light curve analysis.

1.3.2 Time series analysis on light curves

Light curves consist of brightness profiles of variable stars as a function of time. This type of data is called time series data. Analysis of light curves involves time series analysis techniques. Time series analysis comprises methods for analyzing time series data in order to extract meaningful statistics and other characteristics of the data. Using time series analysis on light curve data, it can be found that how many pulsations are present in the star, their pulsation periods and amplitudes.

Light curve contains amplitude vs. time data. It's called the time domain. To extract meaningful information, time domain should be converted to the frequency domain which is a power vs. frequency plot. It's also called frequency spectrum. There are several mathematical techniques to do this kind of a time-series analysis. Commonly used time series analysis techniques in the study of variable stars are Fourier Transformation(FT) and Least Square spectral analysis also known as Lomb-Scragle method(LS Method).

1.3.3 Discrete Fourier transformation method

Discrete Fourier transformation is the most popular frequency analysis technique. Fourier transformation decomposes a function of time into frequencies that make it up. Applying Fourier transformation to light curve data returns the frequency spectrum which consist of details about pulsations (or periodicities) in the light curve.

$$P_\omega = \sum_{n=0}^{N-1} x_n . e^{-\frac{j2\pi\omega n}{N}} \tag{1.11}$$

Main drawback of this method is its accurate only if constant sampling frequency is maintained. But in astronomical studies it's very difficult to maintain a constant sampling frequency due to weather conditions, atmospheric variations clouds and etc. If the sampling frequency is not constant, Fourier transformation method will take the average sampling frequency over the full range of data, into account.

1.3.4 Least squares spectral method

As discussed in the previous section, Fourier transformation as well as most of the other standard methods available for frequency analysis, are accurate only if a constant sampling ratio can be maintained. In other words, for data obtained at uniformly spaced intervals. But in practical astronomy, it's very hard to obtain uniformly spaced data. Observations are limited to night time unless it's a solar observation. Observations are also restricted by the weather, availability of telescope time and the celestial position of the object under observation. The frequency spectrum of non-uniform time-series data is far more complicated than uniform time-series data. Each true peak in the spectrum gives rise to a number of other peaks of varies heights which are called aliases.

One of the common methods of calculating the spectrum of non-equally spaced data is periodogram analysis. In this method, frequency analysis is performed ignoring non-uniformity of data, assuming that data is equally spaced with average sampling frequency, therefore contain some error. The least square spectral method is an extension of Fourier transformation which can be used to analyze non-uniform data. It provides the best power spectrum from non-uniformly spaced time series data. It reduces to the Fourier power spectrum in the limit of equal spacing. The least square spectral analysis is also known as Lomb Scragle method based on the contributions of Nicholas R. Lomb [19] and, independently, Jeffrey D. Scargle.[20]

The periodogram at frequency ω is defined as,

$$P_X(\omega) = \frac{1}{2}\left\{\frac{\left[\sum_j X_j \cos\omega(t_j\text{-}\tau)\right]^2}{\sum_j \cos\omega(t_j\text{-}\tau)^2} + \frac{\left[\sum_j X_j \sin\omega(t_j\text{-}\tau)\right]^2}{\sum_j \sin\omega(t_j\text{-}\tau)^2}\right\} \qquad (1.12)$$

Where the time delay τ is defined as,

$$tan2\omega\tau = \frac{\sum_j sin2\omega t_j}{\sum_j cos2\omega t_j}$$
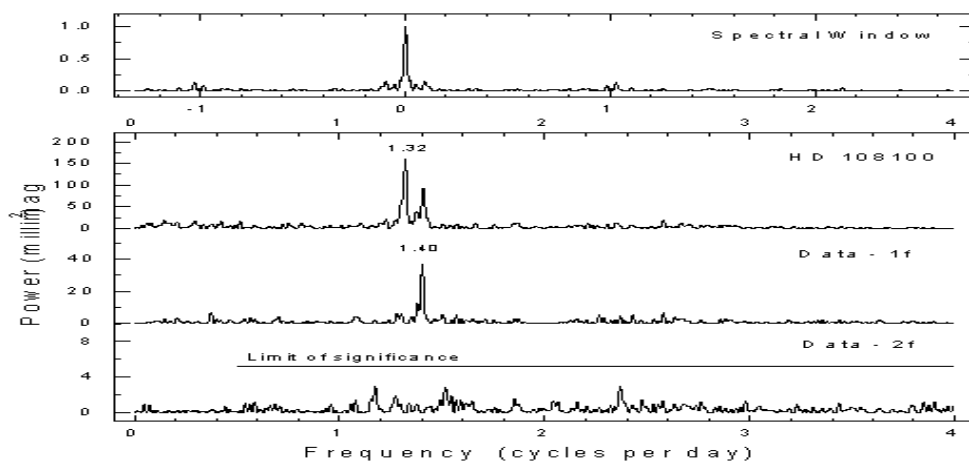
Figure 1.12 Frequency spectrum of variable star HD 108100 [21]

1.3.5 Light curve analysis using VARTOOLS

The VARTOOLS is a command line utility that provides tools for processing and analyzing astronomical time series data. It includes methods for calculating variability and periodicity statistics of light curves; for filtering, transforming, and otherwise modifying light curves; and for modeling light curves. It is intended primarily for batch processing a large number of light curves. The program is run by issuing a sequence of commands to perform actions on light curves, each command is executed in turn with the resulting light curves passed to the next command. Statistics computed by each command are stored in ASCII format. [22]

VARTOOLS is a free and open source program developed by a group of astronomers at the Princeton University. The development of VARTOOLS is supported by a NASA grant. It has been successfully used in many variable star astronomy research including space astrometry missions like Hipparchus, CoRoT, Kepler etc.[23] VARTOOLS runs on many of the Linux operating systems. It requires some additional programs available for Linux which are developed specially for research purposes.

In this study, light curve analysis was done using the VARTOOLS program. Normalization of light curves, converting light curves into phase amplitude diagrams, performing least square spectral analysis and discrete Fourier transformation on light curves were done. The following table shows the VARTOOLS commands used for certain tasks. Refer the Appendix D for the codes.

Table 1.3

VARTOOLS Commands used for light curve analysis

Task	VARTOOLS Command
Least Square spectral analysis	LS
Discrete Fourier transformation	dftclean
Conversion of light curves into Phase amplitude	phase

CHAPTER 2

METHODOLOGY

2.1 Equipment

2.1.1 Reflection Telescopes

Telescopes are the primary and main equipment used in astronomical observations. It is also true in the case of variable star astronomy. In photometry, telescopes are used to gather light from the object under observation. There are two main categories of telescopes according to the behavior of light inside them. Refraction telescopes use lenses to control light while reflection telescopes use lenses and mirrors. Images produced by the refraction telescopes are affected by many optical distortions such as chromatic aberration and spherical aberration. Modern reflection telescopes use parabolic mirrors to successfully reduce those distortions. Since there are low optical distortions, reflection telescopes are better than refraction telescopes in scientific observations.

Reflection telescopes are categorized into two main groups depending on their configuration. Newtonian reflection telescopes use a flat mirror as the secondary mirror while cassegrain reflection telescopes use a hyperbolic mirror. Reflection telescopes have successfully reduced chromatic aberration and spherical aberration by using parabolic mirrors, but it leads to another optical distortion called comatic aberration or Coma which is distorted images appearing to have a tail like a comet. In cassegrain reflection telescopes, comatic aberration was successfully reduced by using the secondary hyperbolic mirror. Therefore, cassegrain reflection telescopes provide better images than Newtonian reflectors, but modern Newtonian telescopes use correction lenses to minimize comatic aberration.

In this study, two telescopes were used. The main telescope used was a 45cm diameter, Cassegrain reflection telescope, located in the observatory at Arthur C. Clark Institute of modern technologies, Srilanka, which was used to obtain images for the star SZ Lyn and the other was a Meade 14" Newtonian reflection ACF LX850 portable Telescope which was used to obtain images of the stars YZ Boo and ZZ Mic.

Figure 2.01 45cm Cassegrain telescope at ACCMT

Figure 2.02 ACF LX850 portable Telescope

2.1.2 CCD Cameras

Charge couple devices or CCDs are semiconductor chips with integrated circuits which are sensitive to incident light and capable of recording incident light patterns into a digital image. With the development of semiconductor technology and electronics, CCDs have become the most important equipment in digital imaging. [24]

A CCD contains an array of photosensitive elements called pixels. These pixels emit electrons when photons are incident on them. CCD electronics, read out those electron charges and record the photon flux values received by each pixel in a digital image. Those images can be analyzed to obtain photometric results of the photographed objects.

In astronomy, those images which to be analyzed, are obtained and stored in uncompressed formats to prevent a loss of data. They are known as raw images. Number of formats are used in storing these raw images but all of them store the flux values in a matrix which dimensions are equal to the dimensions of the CCD sensor. In other words each matrix element corresponding to a pixel in the CCD. The element value is the received flux by the particular pixel. Therefore, it's able to perform arithmetic operations (Especially matrix algebra) on pixel values. Image analysis is basically done by these arithmetic operations. [25]

Other than the matrix, these raw images also contain the some other useful information such as the time of observation, exposure time of the image, CCD temperature, filters used for observations, etc. These information are known as header data. In the header, history flags can be stored which make the analysis steps reversible even if the images are overwritten.
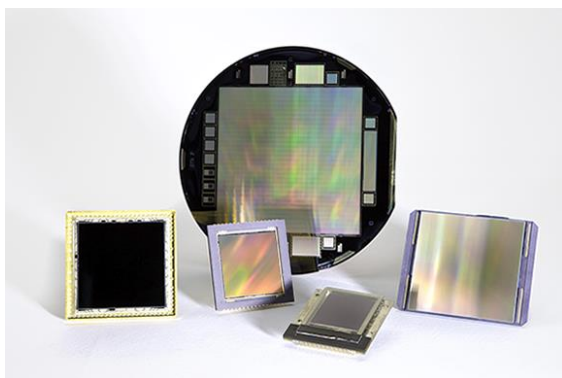
Figure 2.03 Photosensitive semiconductor chips in CCDs

Figure 2.04 Apogee Alta F9000 CCD Camera

2.1.3 Filter Systems

In astronomical observations, filters are used often. Filters pass a certain band of wavelengths through them while the light of other wavelengths are blocked. Therefore, filters can be used to determine the color dependence or wavelength dependence of the incident flux. By understanding the color dependence, very important conclusions can be made. Johnson-Cousin filter system is the commonly used filter system in astronomy. In Johnson-Cousin filter system, filters are indicated by letters. [26]

Table 2.1

Central-Band wavelengths of Johnson-Cousin filters [27]

Filter	Central-Band wavelength (nm)
U	365.6
B	435.3
V	547.7
R	634.9
I	879.7
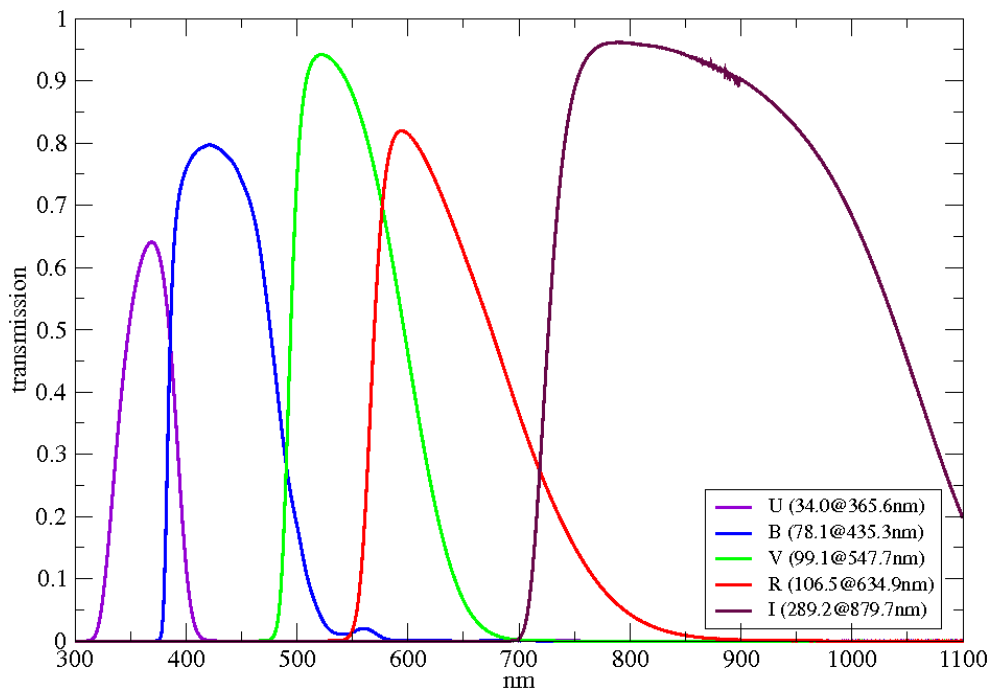
Figure 2.05 Transmission curves of Johnson-Cousin filters [27]

2.2 Image analysis using IRAF

2.2.1 Introduction to IRAF

Image Reduction and Analysis Facility AKA IRAF is a free and open source collection of software written by the National Optical Astronomy Observatory, USA (NOAO). It was created to perform photometry primarily from data taken from CCD cameras. It provides a platform and a programmable environment for digital image analysis. It runs on Linux operating systems. IRAF is written using C and FORTRAN computer languages. IRAF commands (known as tasks) are organized into package structures. Additional packages may be added to IRAF. It is the most used image analysis software in the field of astronomy. [28] In this study, all the image analysis was done using the IRAF. Refer Appendix A for the codes.

2.2.2 Image alignment and shift

In this study, nearly 3500 images were analyzed and images were taken throughout a long time period. Since telescopes have tracking imperfections, in long image sequences, photographed objects show movements through the images. Therefore, it can't be set a single location for the objects in the images (In this case, variable star, comparison star and check star), for all images. Also, it is impossible to perform the analysis for whole set of images manually. Best way is to shift and align the images so it can be set single locations to all objects in each image and program the IRAF to do the analysis to these locations (objects).

First, the obtained images were grouped by the filter applied. Then, in each group, images were sub grouped so that each sub group contains 50 images. Within a sub group the star field showed an approximately liner movement. Therefore, by calculating the vertical and horizontal gradients of this linear motion, an IRAF script were written to shift and align all images in the sup group. All images were aligned by applying the same procedure for all sub groups.

IRAF task imshift which allows to shift images was used in this process. Refer Appendix B for the codes and the parameters used in the IRAF task imshift.
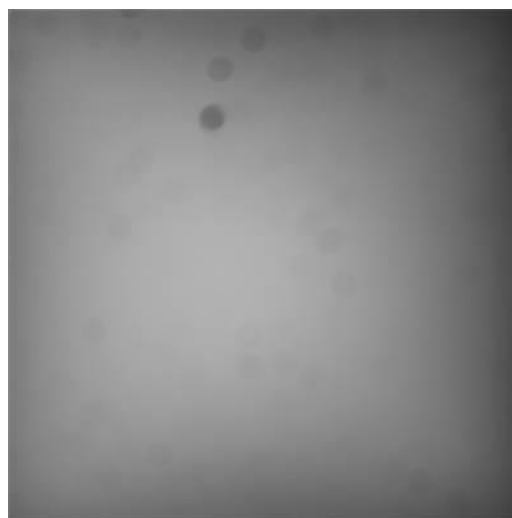
Figure 2.06 The master flat frame for V Band (some pixel to pixel variations can be seen)

2.2.3 Dark and Bias subtraction

Before obtaining photometric measurements, it's necessary to remove artifacts and noises which are not generated by photons from the images. The main artifacts can be seen in the CCD images are the noises due to dark current and bias current. To activate the CCD, a voltage must be applied and this voltage known as the bias voltage. Because of the bias voltage, always there is a small current called the bias current. Flux values recorded in the images also contain the electron flux due to bias current. Also, when the semiconductor devices (CCD) heat up, thermally excited electrons contribute to the current. Therefore, obtained images contained a noise due to thermally excited electrons and the bias current. Since these noises are added to the images, this is known as an additive error.

To eliminate the effect from the above explained noises, some images were obtained with closed shutter but with the same exposure time of science frames (Images which contain the objects which to be performed the photometry). These images are known as Dark frames. Since the shutter was closed, no photons were incident on the CCD. Therefore these obtained images had the flux values generated only from thermally excited electrons and the bias current. Combining those dark frames, an average dark frame called master dark, was created. Then the master dark was subtracted from each image to eliminate noise from the images.

In some advanced telescopes, CCDs are cryogenically cooled to very low temperatures using liquid nitrogen. In these temperatures, contribution from the thermally excited electrons is negligible and no dark subtraction is needed. But the CCD isn't cryogenically cooled at the time of observation, it may be need to perform dark subtraction from the images before photometric measurements. Since, bias current is always present in the CCD bias subtraction is always required.

IRAF is integrated with tasks (commands) which allow to combine dark frames to create the master dark and to perform dark subtraction on science frames. IRAF task 'darkcombine' was used to create the master dark frame. The master dark is showed in the figure-05.Refer appendix for the codes and the parameters used in IRAF task darkcombine.
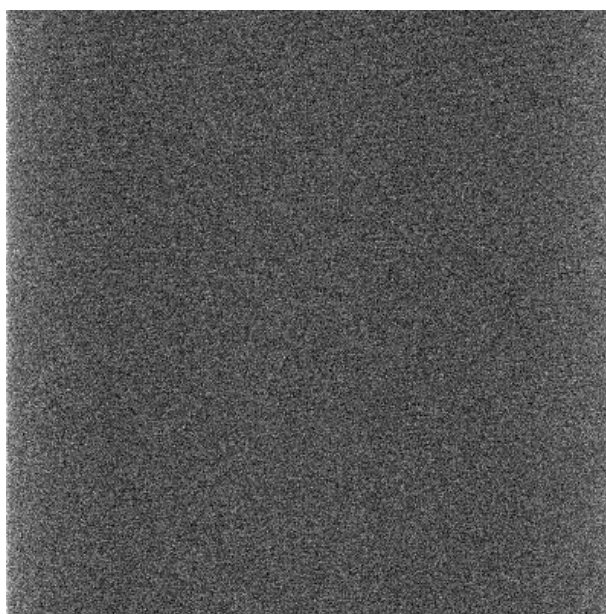
Figure 2.07 The master dark frame for Band V (white dots are the noise thermal electrons and bias current)

2.2.4 Flat field correction

CCDs are fabricated using very advanced technology. But there is a possibility that the CCD contains defects and impurities. Also, there may be dust particles accumulated on the CCD or filters as stains. Because of these reasons, every pixel in the CCD may not be equally sensitive to the light but may have pixel to pixel variations in light sensitivity. Since the flux values are multiplied by pixel sensitivities to light, this is called multiplicative error.

To eliminate pixel to pixel variations, Flat frames must be obtained. A flat frame is an image obtained by uniformly illuminating the CCD. This uniform illumination can be done by projecting a white light to the observatory dome (dome flats) or by exposing the CCD to the twilight (Twilight flats).

The flat frame can be normalized by dividing each flux value by the mode of the flux values within the image. Therefore, normalized flat frames reflect a pixel sensitivity map of the CCD. By dividing the image by the flat frame, pixel to pixel variations can be eliminated from the image.

2.2.5 Image reduction procedure

Preparing the images for magnitude measurement by removing noises and eliminating pixel to pixel variations is called image reduction. Image reduction is basically done by performing dark subtraction and flat field correction. Image reduction procedure can be summarized as follows.

$$Reduiced\ frame = \frac{Raw\ frame - Master\ dark\ frame}{Master\ flat\ frame} \qquad (2.01)$$

Here,

$$Master\ dark\ frame = \sum_{i,j} \frac{\sum_{k=1}^{n} Flux_{i,j}^{k}}{n}$$

$$Master\ flat\ frame = \sum_{i,j} \frac{\sum_{k=1}^{n} Flux_{i,j}^{k}}{n}$$

Where,

N   - Number of dark frames or flat frames
i,j   - Refer a pixel at i^{th} column and j^{th} row

Table 2.2

Image reduction and analysis procedure

Raw images
Dark frames · Science Frames (Raw Frames) · Flat Frames

↓

Combining Flats and Dark
Master Dark · Master Flat

↓

Dark Subtraction and Flat Correction
Dark Substracted and Flat corrected Science Frames

↓

Aligning Images
Aligned Images to the common coordinates

↓

FWHM calculation
creating the radial profile of the stars · suggesting the apature radiaus for photometry

↓

Measuring the Magnitudes
Intrumental magnitudes and Mag. errors

↓

Extraction of Julian Dates of observation
Julian Dates of observation

↓

Plotting the Light Curve
Light curves of each colour band

↓

Time series analysis
Fourier analysis · Least-Squre spectrum analysis

↓

Pulsation Periods

2.2.6 Magnitude Calculation using PHOT

When an image of a star is taken by the CCD, light from the star is spread over a number of pixels. To calculate the magnitude of the star from the image, all the flux values in these pixels must be added up and the average background flux must be subtracted from that. In order to perform this, an aperture and an annulus co-centric the star can be defined as show in the figure 2.8. Then flux values within the aperture can be added up and subtracted by the background flux which is determined by the flux values within the annulus. To collect maximum light from the star, usually the aperture radius is defined as 3.5 times of the full width of the half maximum (FWHM) of the radial profile. [29] FWHM can be found by plotting the radial profile of the star using the IRAF task phot
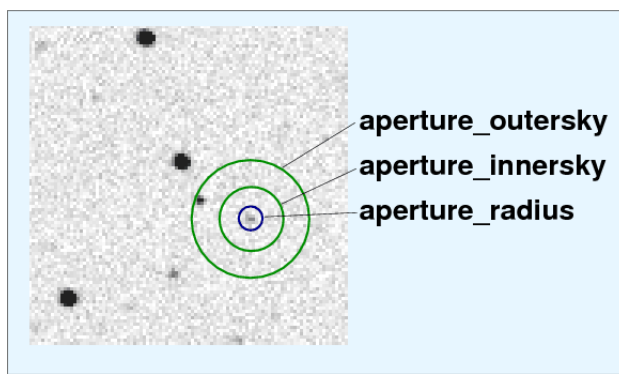
| Figure 2.08 Aperture and sky annulus | Figure 2.09 Cross-sectional intensity variation |

'Phot' is an IRAF task which allows to calculate magnitudes of a star (or any celestial objects) in digital images using aperture photometry. It uses the following formula to calculate the instrumental magnitude of stars.

$$\text{Instrumental magnitude}(m) = -2.5\log(\frac{N_{ap} - A_{ap}.S_{sky}}{t_{exp}}) \qquad (2.02)$$
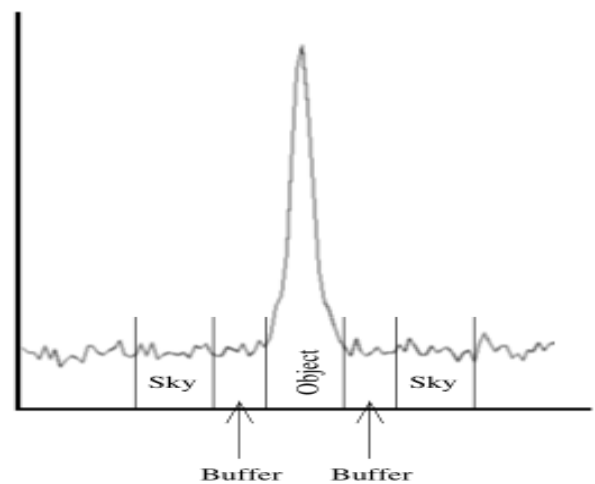
Where,

N_{ap} - Total counts in aperture
A_{ap} - Area of the aperture in pixel^2
S_{sky} - Background flux per unit area
t_{exp} - Exposure time

Generally, a calibration should be done to convert instrumental magnitudes into standard magnitudes. But in this study, differential photometry method was used and therefore, calibration constants are canceled out as discussed in an above chapter. Therefore, no calibration is needed.

By performing the IRAF task 'phot' in the batch mode, magnitudes of stars can be calculated. See the Appendix C for the code.
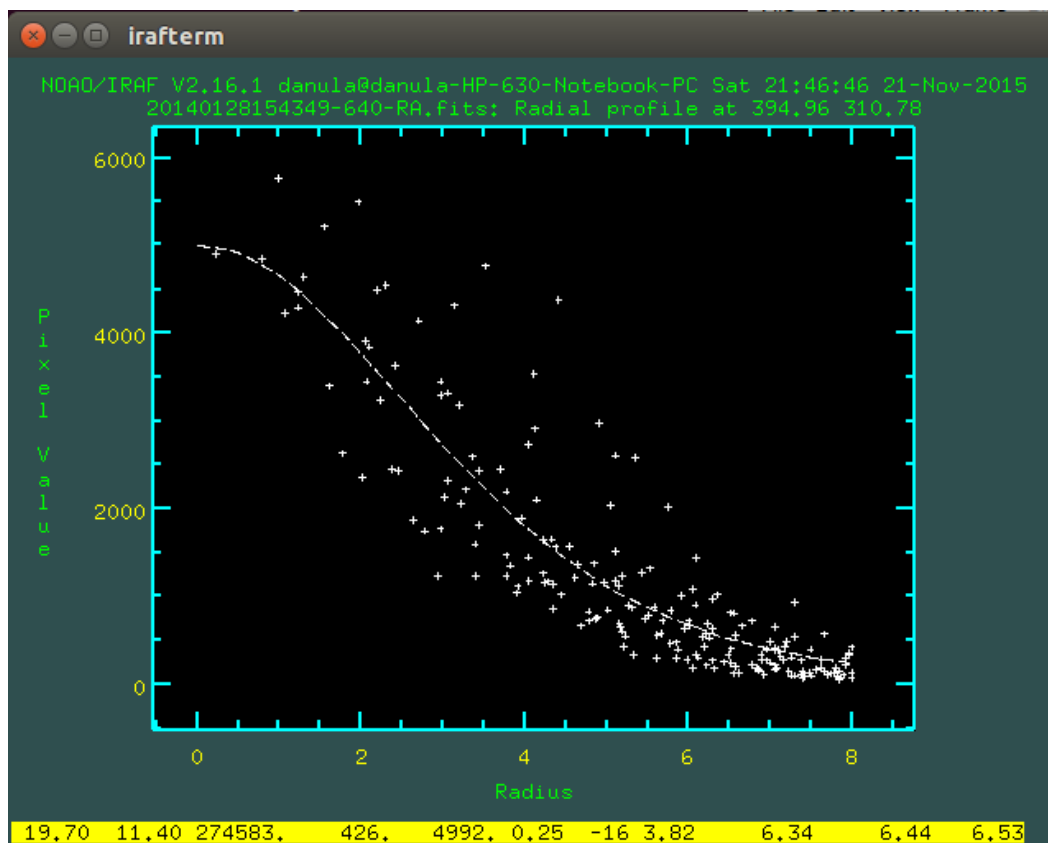
Figure 2.10 Radial profile of the star SZ Lyn (Band V)
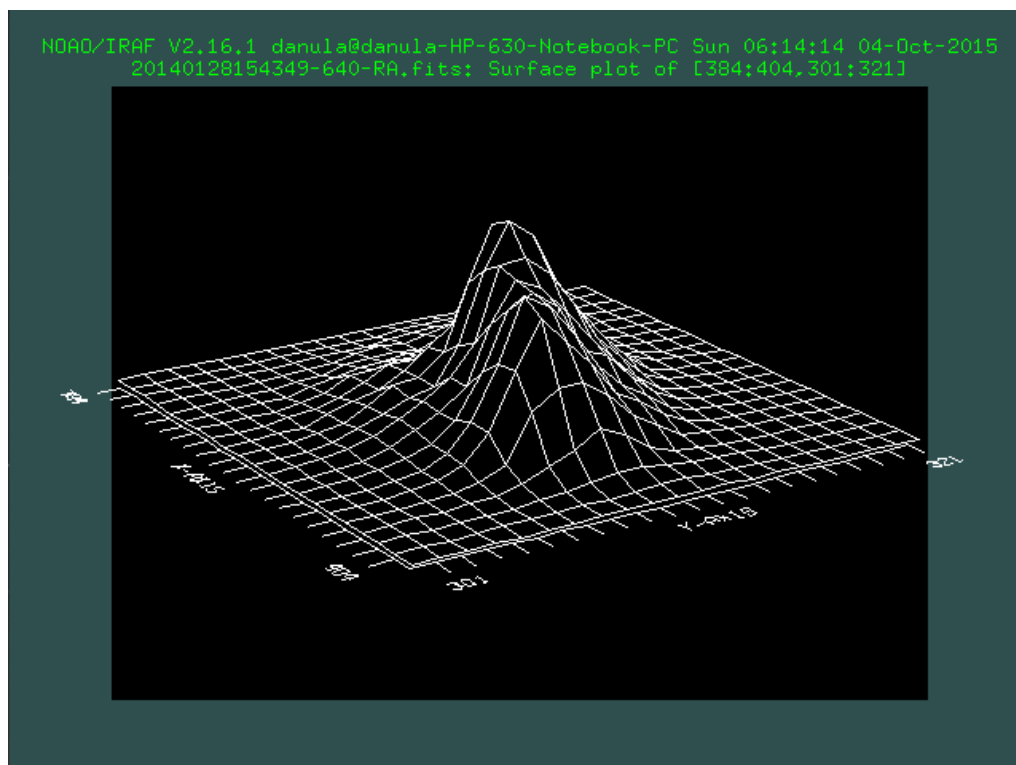
Figure 2.1l surface plot of the star SZ Lyn (Band V)

CHAPTER 3

RESULTS AND ANALYSIS

3.1 Light curve Analysis of SZ Lyn
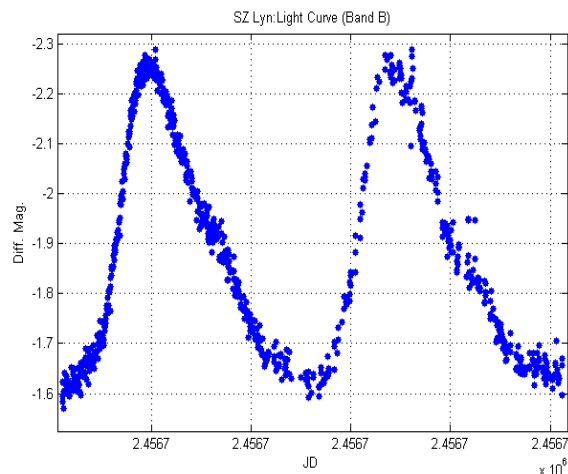
Figure 3.0l Light Curve of SZ Lyn (Band B)
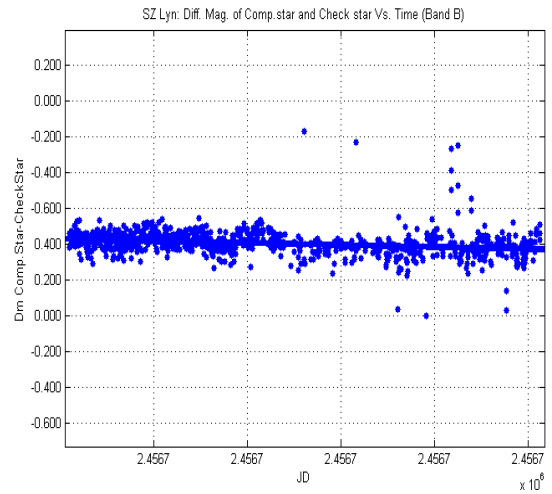
Figure 3.02 The graph of mag$_{comp.}$-mag$_{check}$ vs. time
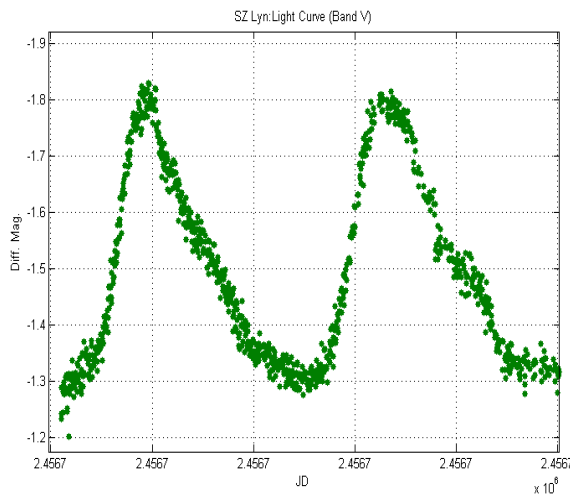
Figure 3.03 Light Curve of SZ Lyn (Band V)
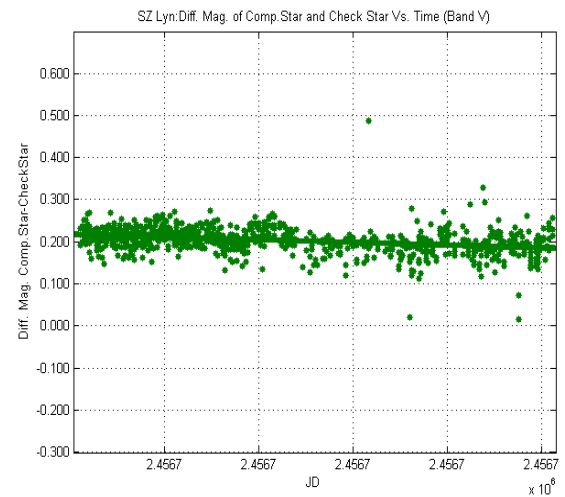
Figure 3.04 The graph of mag$_{comp.}$-mag$_{check}$ vs. time
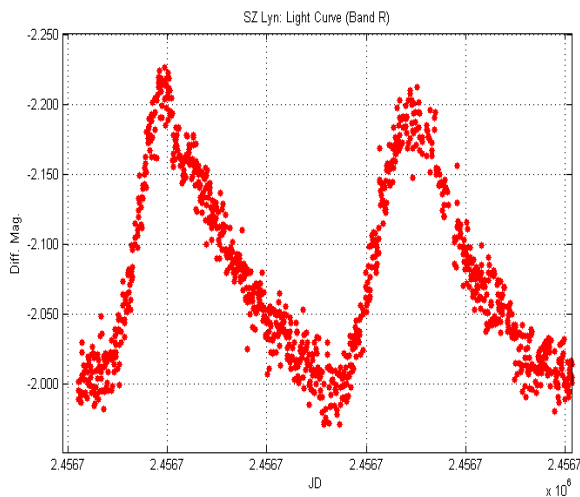
Figure 3.05 Light Curve of SZ Lyn (Band R)
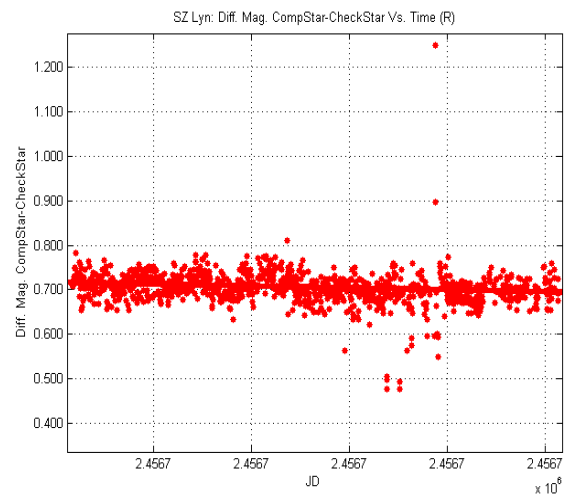
Figure 3.06 The graph of mag$_{comp.}$-mag$_{check}$ vs. time

Obtained light curves of SZ Lyn are shown in the figures 3.01-3.06. The graphs of differential magnitude of check star and comparison star vs. time were used to check whether that check star and comparison star are non-variable. Since the differential magnitudes were constant with time (gradients were very close to zero), it was found that check star and comparison star are non-variable.
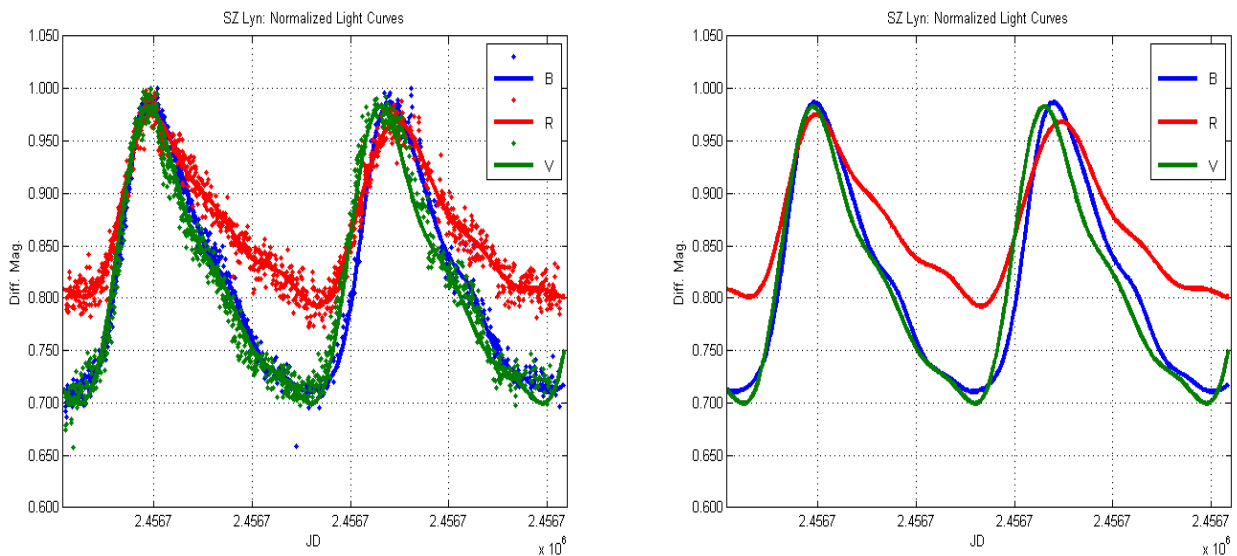
Figure 3.07 Normalized light curves of SZ Lyn

Three light curves (Band B,V and R) were normalized at the peaks and a Fourier fit was applied to compare the color dependence of the magnitude variations. It was clearly observed that amplitude variation in the R band is significantly lower than B and V bands (Figure 3.7).

The color indexes, B-V and V-R were calculated at the maximum and minimum brightness's of the light curves of SZ Lyn. Since the color index is corresponding to blackbody's color (In this case star), changes in the color index at the peaks and valleys of the light curve concludes that the star (SZ Lyn) goes through a color change while the brightness changes from maximum to minimum. By examining the color indexes it can be concluded that the star (SZ Lyn) appear bluer at the highest brightness and redder at the lowest brightness. Therefore, from the blackbody radiation it can be further concluded that star (SZ LYN) has a higher surface temperature at the maximum brightness and lower surface temperature at the minimum brightness. Also, by considering the temperature gradient of a star from the center to the surface it can be concluded that the star (SZ Lyn) is contracted when the maximum brightness occurs and expanded when the minimum brightness occurs.

Table 3.1

Color indexes of SZ Lyn at maximum and minimum brightness

Color Index	At Maximum	At Minimum
B-V	-0.460	-0.295
V-R	0.424	0.700

The difference of amplitude variation between R band and B, V bands can be explained by the fact that very large visual amplitudes are not due to large luminosity changes, but due to a shifting of energy output between wavelengths as the stars change surface temperature during their pulsations.
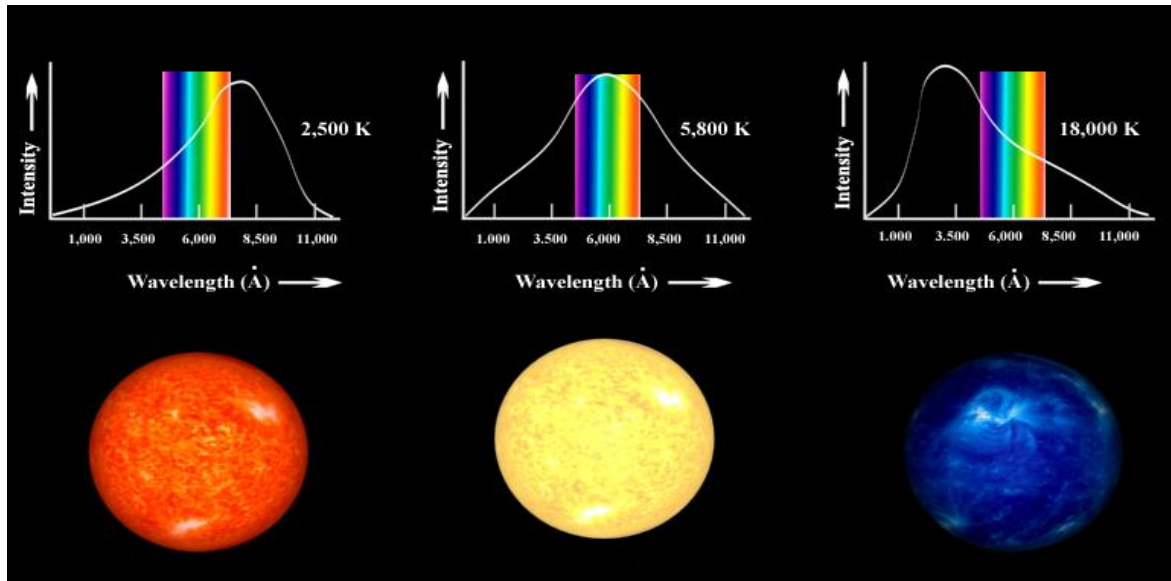
Figure 3.08 Shape of blackbody curves of stars with different visual colors [30]

The shapes of the blackbody curves of a red star, a yellow star and a blue star are shown in the figure 3.08. Also, the visual range of the electromagnetic spectrum is shown in the blackbody curves. In a blue star like SZ Lyn, by examining the gradient of the blackbody curve, it can be shown that a small wavelength shift near blue wavelengths cause a large intensity variation but the same wavelength shift near red wavelength will cause relatively low intensity variation. This explains the difference of brightness variation between R band and B,V bands.
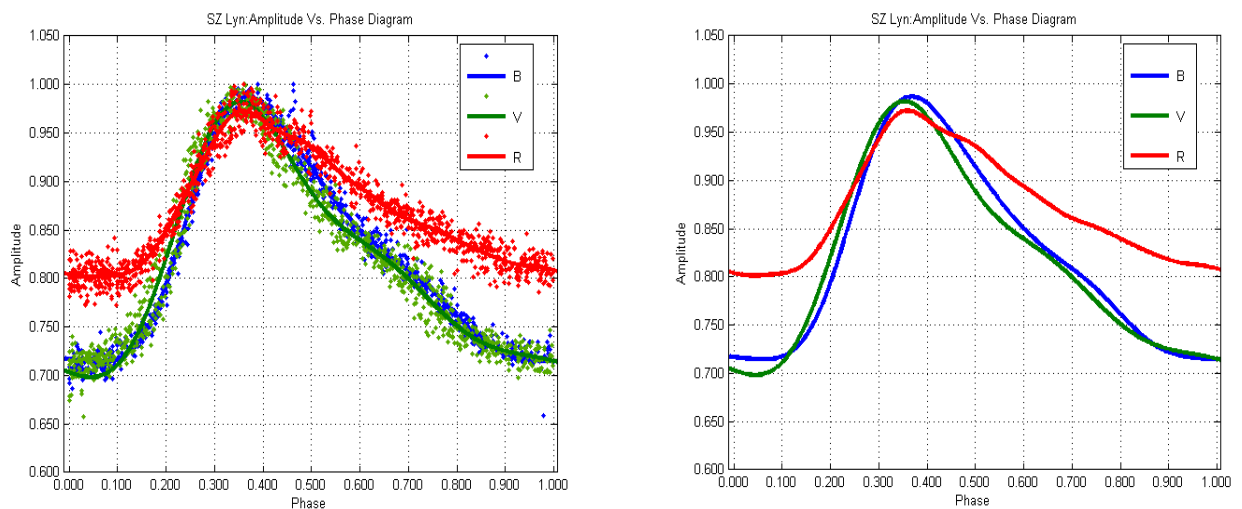
Figure 3.09 The graph of phase vs. amplitude of SZ Lyn for band B,V and R

Phase amplitude diagrams were obtained by converting the time axis of light curves in to the phase. They clearly show the asymmetricity of the light curves of SZ Lyn. By observing the phase amplitude diagram it can be conclude that Delta Scuti stars are contracting faster than they expand.

3.2 Frequency Analysis of SZ Lyn

Frequency analysis was done using least square spectral method and discrete Fourier transformation method. Frequency spectrums obtained from both methods for each band are shown below. For SZ Lyn, Three pulsations were detected using both methods.

Least Squre spectral analysis   **Fourier tranformation**
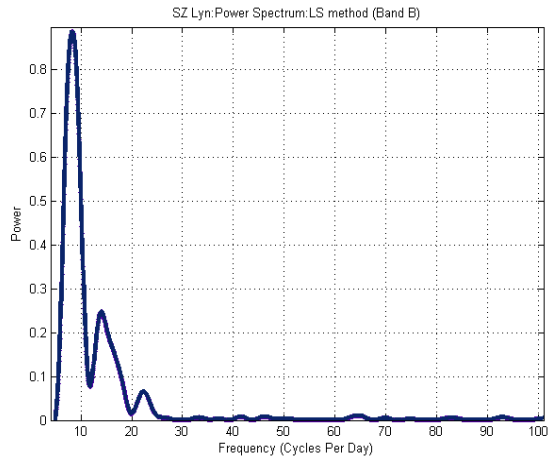
Figure 3.10 SZ Lyn (Band B): LS method
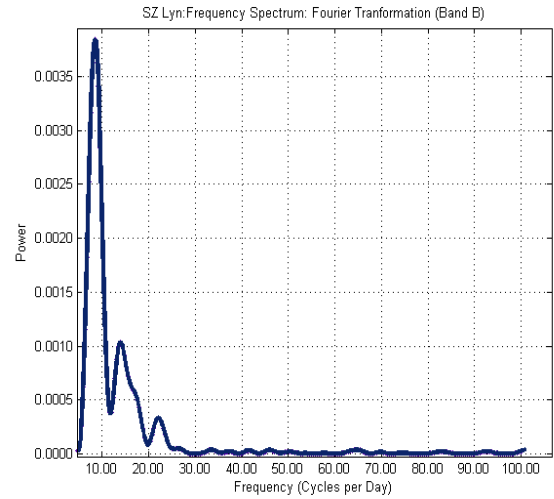
Figure 3.11 SZ Lyn (Band B): FT
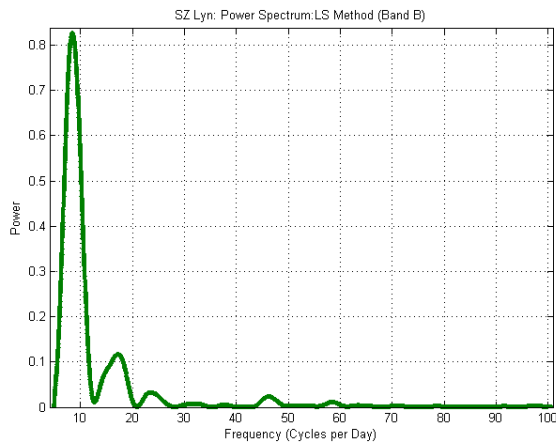
Figure 3.12 SZ Lyn (Band V): LS method
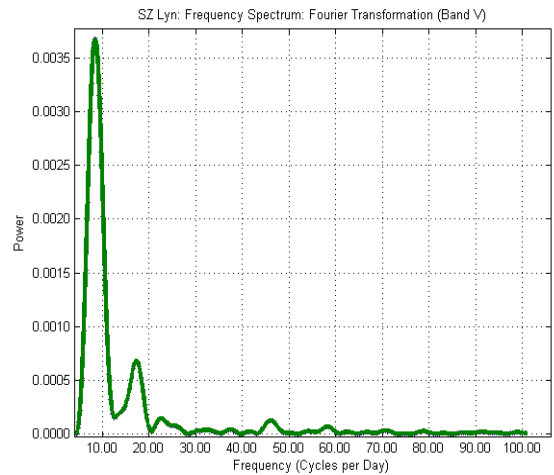
Figure 3.13 SZ Lyn (Band V): FT
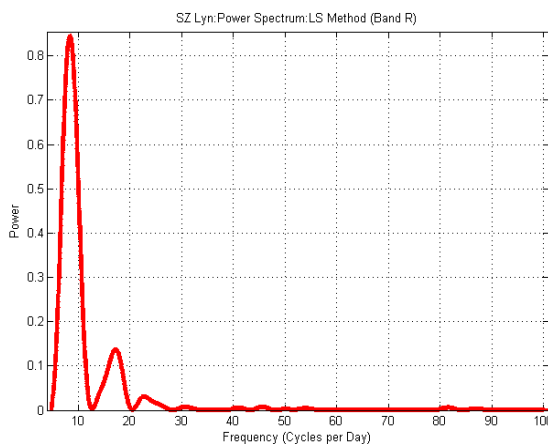
Figure 3.14 SZ Lyn (Band R): LS method
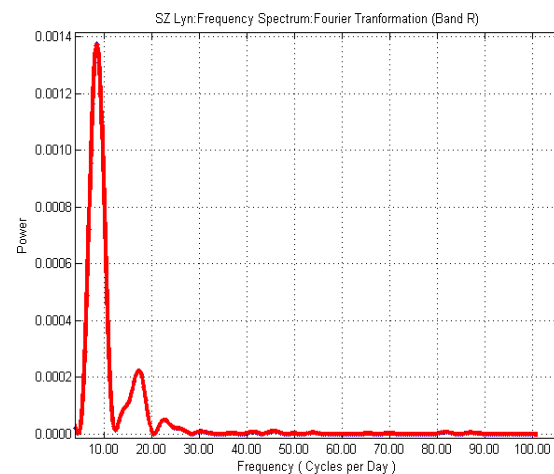
Figure 3.15 SZ Lyn (Band R): FT

Table 3.2

Pulsation periods of three pulsations of SZ Lyn

Pulsation	Band B		Band V		Band R	
	LS	FT	LS	FT	LS	FT
P_0 (Days)	0.1201	0.1195	0.1186	0.1171	0.1195	0.1195
P_1 (Days)	0.0607	0.0717	0.0585	0.0572	0.0608	0.0584
P_2 (Days)	0.0406	0.0456	0.0395	0.0439	0.0408	0.0439
P_1/P_0	0.505	0.600	0.493	0.488	0.509	0.489
P_2/P_0	0.338	0.382	0.333	0.375	0.341	0.367
P_2/P_1	0.669	0.636	0.675	0.767	0.671	0.752

Fourier transformation was used just as a confirmatory method, since least square spectral method is more accurate (for non-uniformly spaced data), the periods obtained from LS method were used in further calculations.

Period ratio, P_1/P_0 is close to 0.687 confirming a high density concentration toward the center as discussed in the chapter-01. It indicate that SZ Lyn consists of two regions of different densities. Generally, stars have heavier elements near the center and lighter elements like H and He at shells (outer layers).

3.3 Estimation of stellar average density and internal structure

Average density of SZ Lyn can be calculated using the 1.05 equation derived in chapter-01.

$$\rho_{avg} \approx \frac{12}{\pi G \gamma P^2}$$

V band in the Johnson-Cousin system covers a wide range of wavelengths in the visual spectrum. Therefore in astronomical calculations, generally the results obtained through the Johnson V band is considered. Therefore, the pulsation period obtained through the Johnson V band using LS method was used to calculate the average density. The ratio of specific heats, ϒ was taken as 5/3 assuming that the star contains monoatomic gas and pulsate adiabatically. Average density of SZ Lyn was calculated to be 327.04 kg m^{-3}.

3.4 Secondary target stars

In this study, Delta Scuti stars, YZ Boo and ZZ Mic were selected as secondary target objects. Photometric analysis for these stars were done using only the Johnson V band and a relatively lower time resolution. Frequency analysis was done using both least square spectral analysis and discrete Fourier transformation. Two pulsations were successfully detected in YZ Boo and only the main pulsation period of ZZ Mic was detected. Other pulsations which might be visual in the frequency spectrum are ignored due to very low false alarm probability and signal to noise ratio (SNR). Results obtained from the frequency analysis are shown in the tables 3.3 and 3.4. Average densities were calculated using the fundamental pulsation periods obtained from LS method.

YZ Boo
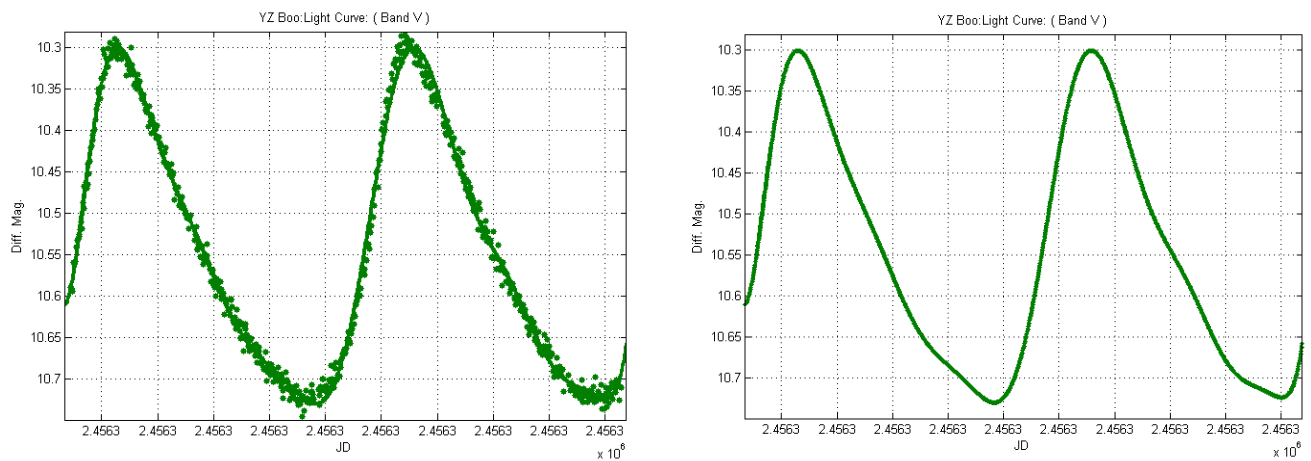
Figure 3.l7 Light Curve of YZ Boo (Band V)
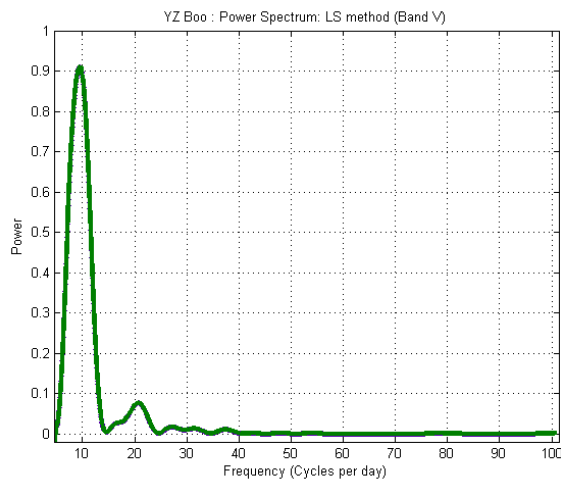
Figure 3.l8 YZ Boo: Frequency Spectrum: LS method   **Figure 3.l9** YZ Boo: Frequency Spectrum: FT
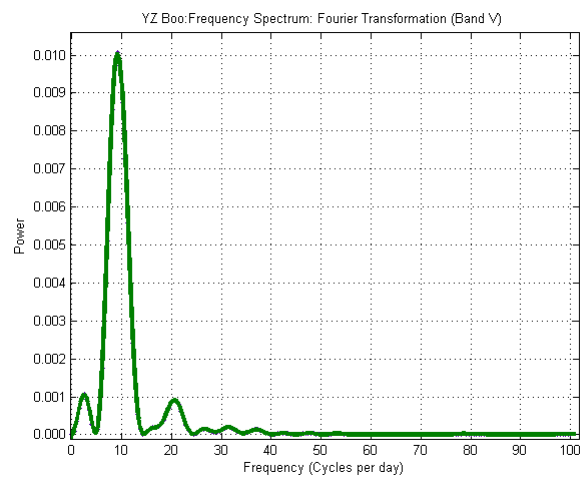
Table 3.3

Pulsation periods of YZ Boo for Band V

Pulsation	LS	FT
P_0 (Days)	0.1052	0.1089
P_1 (Days)	0.0482	0.0490
P_1 / P_0	0.458	0.450

ZZ Mic
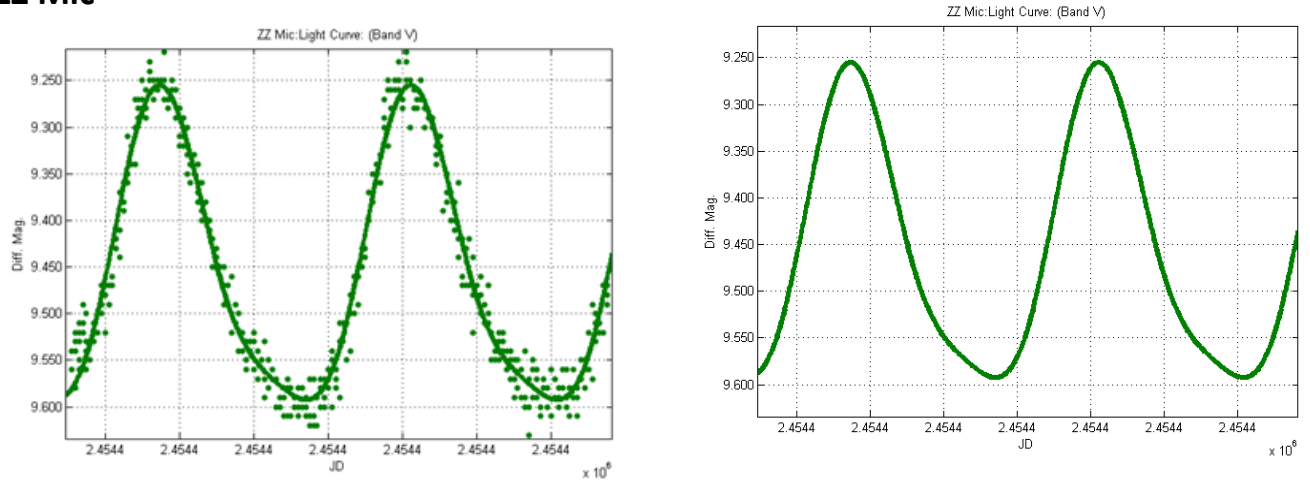
Figure 3.20 Light Curve of ZZ Mic (Band V)
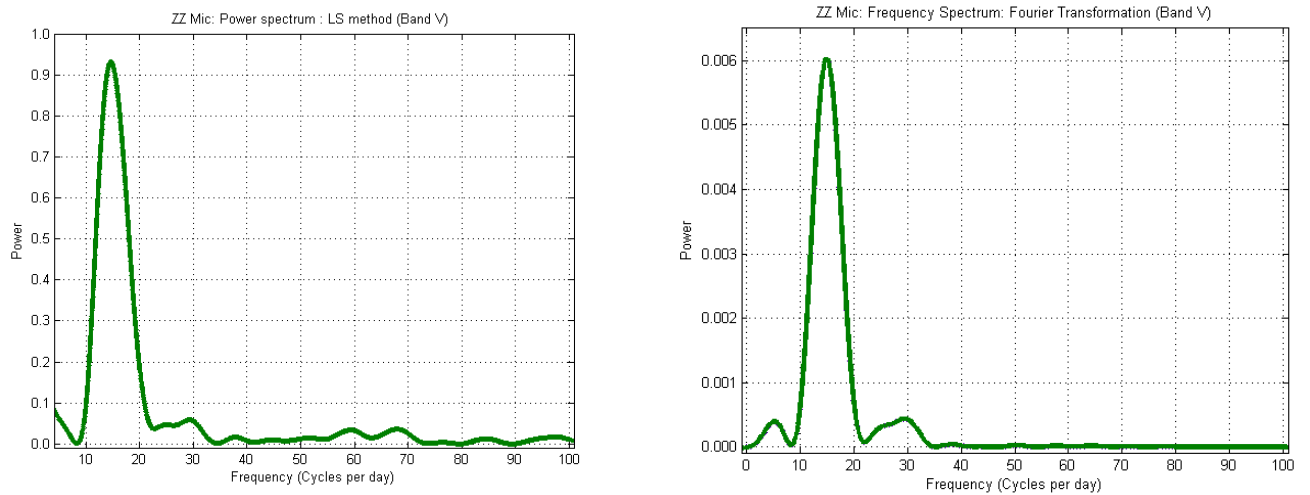
Figure 3.21 YZ Boo: Frequency Spectrum: LS method   **Figure 3.22** YZ Boo: Frequency Spectrum: FT

Table 3.4

Pulsation periods of ZZ Mic for Band V

Pulsation	LS	FT
P_0 (Days)	0.0681	0.0686

3.5 Conclusions

Table 3.5

Summary of Results

Star	Detected pulsations	Main Pulsation Period (Days)		Average density (kg m⁻³)
		Experimental	IVSI Catalog [31]	
SZ Lyn	3	0.1186	0.1205	327.04
YZ Boo	2	0.1052	0.1041	415.66
ZZ Mic	1	0.0681	0.0672	991.92

It was clear that differential photometry was the most effective and convenient method to perform light curve analysis of variable stars. By using this method, not only long and time consuming calibration processes such as airmass calculation, standard magnitude calibrations were dropped from the experimental procedure but also made the results more reliable. It was found that Delta Scuti stars go through a color change during the pulsations and it is caused by mainly the change of surface temperature during pulsations. Also, it was experimentally found that in pulsating variables, generally the amplitude variation shown in the R band is smaller than that of in the B and V bands which can be explained by blackbody radiation and Wien's law. Furthermore, it was concluded that Delta Scuti stars are contracted at their highest brightness and expanded at their lowest brightness by considering the temperature gradient of stars from the center to the surface.

Three vibrations were detected in the variable star SZ Lyn, which were found that the fundamental vibration and two harmonics. Period ratios of these pulsations indicate that SZ Lyn has a higher density profile towards the center. Average densities of stars were calculated using the Eddington's period-density relationship. Even though, there wasn't records of previous research contain average density results of these Delta Scuti stars, obtained results were consistent with a previous research which carried out for another set of Delta Scuti stars. [32] As for further research, Obtained period ratios can be used to make further important conclusions about the stellar structure and evolution using computational models.

Main pulsation periods of variable stars, YZ Boo and ZZ Mic were calculated. Results were consistent with pervious research. Two pulsations were detected in YZ Boo and only the main pulsation period was successfully detected in ZZ Mic. Some peaks which were present in the frequency spectrums were ignored due to very low signal to noise ratio. Other pulsations could be successfully detected if the photometric data were obtained with high time resolution as in case of SZ Lyn.

REFERENCES

1. Saladyga M. American association of variable star observers. Variable stars [Online] 2013. https://www.aavso.org/variables-what-are-they-and-why-observe-them [Oct 2015]
2. Porceddu, S. , Jetsu, L.; Lyytinen, J.; Kajatkari, P.; Lehtinen, J.; Markkanen, T; et al. (2008). "Evidence of Periodicity in Ancient Egyptian Calendars of Lucky and Unlucky Days".Cambridge Archaeological Journal 18 (3),p. 327–339.
3. Fontaine G. , Wesemael F. Encyclopedia of Astronomy and Astrophysics, ed. Paul Murdin, Bristol and Philadelphia: Institute of Physics Publishing and London, New York and Tokyo: Nature Publishing Group, 2001, P. 3525
4. Dordonezb. Stellar Variability. [Online]. Photometry. The Astronomical Observatory Of The University Of Geneva, http://obswww.unige.ch/Research/variability/ [Oct 2015]
5. Aerts C. Christensen J. Kurtz D. Astroseimology. Sprinter, 2009, P. 14
6. Brown T. Gilliland R. (1994). "Asteroseismology". Annual Review of Astronomy and Astro-physics,P.32
7. SIMBAD Astronomical Database [Online] 2012. http://simbad.ustrasbg.fr/simbad/ [Oct 2015]
8. Aerts C. Christensen J. Kurtz D. Astroseimology. Sprinter, 2009, P. 22-24
9. Rowe J. Direct imaging photometry with MOST satellite [Online] 2006. http://adsabs.harvard.edu/full/2006MmSAI..77..282R [Oct 2015]
10. SIMBAD Astronomical Database [Online] 2012. http://simbad.u-strasbg.fr/simbad/sim-id?Ident=GCVS%20SZ%20Lyn [Oct 2015]
11. Leavitt H. Pickering, Edward C. Harvard College Observatory Circular, vol. 173, P. 1-3
12. Budge G. An improved Henyey method for calculating stellar models. [Online] 1987. http://adsabs.harvard.edu/full/1987ApJ...312..217B [Sep 2015]
13. Toomer G. , Jones J. "Hipparchus" (1978)
14. Mehra J.; Rechenberg H. (1982). The Historical Development of Quantum Theory. New York: Springer-Verlag. Chapter 1, P. 9-10
15. Wien's displacement law [Online] 2006. https://en.wikipedia.org/wiki/Wien%27s_displacement_law#/media/File:Wiens_law.svg [Oct 2015]
16. Sunlight [Online] https://en.wikipedia.org/wiki/Sunlight#/media/File:Solar_spectrum_en.svg [Oct 2015]
17. Mutlaq J. Star colors and temperatures [Online]2010 https://docs.kde.org/trunk5/en/kdeedu/kstars/ai-colorandtemp.html [Nov 2015]
18. Julian Date Converter [Online] 2013. http://aa.usno.navy.mil/data/docs/JulianDate.php [Sep 2015]
19. Lomb R. (1976). Least-squares frequency analysis of unequally spaced data. Astrophysics and Space Science,vol 39, P. 447–462
20. Scargle D. (1982). Studies in astronomical time series analysis. II - Statistical aspects of spec-tral analysis of unevenly spaced data. Astrophysical Journal vol 263, P. 835.

21. Breger, M., Handler, G., Garrido, R., Audard, N., Beichbuchner, F., Zima, W. A new Gamma Doradus star, HD 108100. [Online] 2010
https://www.univie.ac.at/tops/CoAst/archive/nl10/chapter_8_f.html [Nov 2015]

22. Jhartman. The VARTOOLS Light Curve Analysis Program [Online] 2008.
http://www.astro.princeton.edu/~jhartman/vartools.html [Oct 2015]

23. 20 years of exoplanents. Jet propulsion laboratory [Online] 2012.
http://planetquest.jpl.nasa.gov/page/missions [Oct 2015]

24. Janesick J (2001). Scientific charge-coupled devices. SPIE Press. P. 4

25. Guide to CCD Photometry. American Association of Variable Star Observers. [Online] 2010.
https://www.aavso.org/ccd-photometry-guide [Oct 2015]

26. Johnson H. , Morgan W. (1953) Fundamental stellar photometry for standards of spectral type on the revised system of the Yerkes spectral atlas. The Astrophysical Journal, vol. 117, P. 313–352

27. Johnson-Cousins UBVRI filter curves. [Online] 2010.
http://www.aip.de/en/research/facilities/stella/instruments/data/johnson-ubvri-filter-curves [Nov 2015]

28. Image Reduction and Analysis Facility. National optical Astronomy Observatory [Online] 2012. http://iraf.noao.edu/ [Sep 2015]

29. Messy P. , A User's Guide to CCD Photometry using IRAF, 1992, P. 19-22

30. Aerts C. Christensen J. Kurtz D. Astroseimology. Sprinter, 2009, P. 367-369

31. International variable star index. [Online] 2004. https://www.aavso.org/vsx/ [Nov 2015]

32. Su´arez J. , Garc´ıa Hern´andez G. , Moya A. , Rodrigo C. , Solano E. , Garrido R. , Rod´on J. , Measuring mean densities of δ Scuti stars with asteroseismology Theoretical properties of large separations using TOUCAN [Online] 2014. http://arxiv.org/pdf/1402.0723v2.pdf [Nov 2015]. P. 6

APPENDIX

APPENDIX A

Image Reduction Procedure

01. The dark frames were combined into a master dark, MasterDark.fits.

cl>imcombine @dark_list dark combine=median
@dark_list contains all the dark frames.

02. The master dark frame, MasterDark.fits was subtracted from all the science frames.

cl>imarith @flat_b_list – bias @flat_b_list
cl>imarith @object_b_list – bias @object_b_list
@flat_b_list contains the flats for the B filter.
@object_b_list contains the object frames for the B filter.
This was repeated for flats and object frames the V filter.

03. The flats frames were combined into a master flat frame, MasterFlat.fits

cl>imcombine @flat_list dark combine=median
@flat_list contains all the flat frames.

04. All the science frames were divided by the master flat frame, MasterFlat.fits

cl>imarith @object_B_list – MasterFlat.fits

APPENDIX B

IARF code parameters

Parameters for imshift task

```
vocl> lpar imshift
input               = ""                 Input images to be fit
output              = ""                 Output images
xshift              =                    Fractional pixel shift in x
yshift              =                    Fractional pixel shift in y
(shifts_file        = "")                Text file containing shifts for each image
(interp_type        = "linear")          Interpolant (nearest,linear,poly3,poly5,spline3
(boundary_typ       = "nearest")         Boundary (constant,nearest,reflect,wrap)
(constant           = 0.)                Constant for boundary extension
(mode               = "ql")
```

Parameters for Phot task

```
vocl> lpar phot
image               = "*.fits"           The input image(s)
skyfile             = ""                 The input sky file(s)
(coords             = "coor1.coo")       The input coordinate files(s) (default: image.c
(output             = "default")         The output photometry file(s) (default: image.m
(plotfile           = "")                The output plots metacode file
(datapars           = "")                Data dependent parameters
(centerpars         = "")                Centering parameters
(fitskypars         = "")                Sky fitting parameters
(photpars           = "")                Photometry parameters
(interactive        = no)                Interactive mode ?
(radplots           = yes)               Plot the radial profiles in interactive mode ?
(icommands          = "")                Image cursor: [x y wcs] key [cmd]
(gcommands          = "")                Graphics cursor: [x y wcs] key [cmd]
(wcsin              = )_.wcsin)          The input coordinate system (logical,tv,physica
(wcsout             = )_.wcsout)         The output coordinate system (logical,tv,physic
(cache              = )_.cache)          Cache the input image pixels in memory ?
(verify             = )_.verify)         Verify critical parameters in non-interactive m
(update             = )_.update)         Update critical parameters in non-interactive m
```

```
(verbose          = )_.verbose)    Print messages in non-interactive mode ?
(graphics         = )_.graphics)   Graphics device
(display          = )_.display)    Display device
(mode             = "ql")


PACKAGE           = apphot
TASK              = datapars


(scale            =1.)             Image scale in units per pixel
(fwhmpsf          =11.5)           FWHM of the PSF in scale units
(emission         = yes)           Features are positive ?
(sigma            = INDEF)         Standard deviation of background in counts
(datamin          = INDEF)         Minimum good data value
(datamax          = INDEF)         Maximum good data value
(noise            = poisson)       Noise model
(ccdread          = )             CCD readout noise image header keyword
(gain             = )             CCD gain image header keyword
(readnoi          = 0.)            CCD readout noise in electrons
(epadu            = 1.)            Gain in electrons per count
(exposur          = EXPTIME)       Exposure time image header keyword
(airmass          = )             Airmass image header keyword
(filter           = )             Filter image header keyword
(obstime          = )             Time of observation image header keyword
(itime            = 1.)            Exposure time
(xairmas          = INDEF)         Airmass
(ifilter          = INDEF)         Filter
(otime            = INDEF)         Time of observation
(mode             = ql)
($nargs           = 0)


PACKAGE           = apphot
TASK              = findpars


(thresho          = 4.)            Threshold in sigma for feature detection
(nsigma           = 1.5)           Width of convolution kernel in sigma
(ratio            = 1.)            Ratio of minor to major axis of Gaussian kernel
(theta            = 0.)            Position angle of major axis of Gaussian kernel
(sharplo          = 0.2)           Lower bound on sharpness for feature detection
(sharphi          = 1.)            Upper bound on sharpness for  feature detection
(roundlo          = -1.)           Lower bound on roundness for feature detection
(roundhi          = 1.)            Upper bound on roundness for feature detection
(mkdetec          = no)            Mark detected stars on the display ?
(mode             = ql)
($nargs           = 0)


PACKAGE           = apphot
TASK              = fitskypars
(salgori          = centroid)      Sky fitting algorithm
```

(annulus	= 25.)	Inner radius of sky annulus in scale units
(dannulu	= 10.)	Width of sky annulus in scale units
(skyvalu	= 0.)	User sky value
(smaxite	= 10)	Maximum number of sky fitting iterations
(sloclip	= 0.)	Lower clipping factor in percent
(shiclip	= 0.)	Upper clipping factor in percent
(snrejec	= 50)	Maximum number of sky fitting rejection iterations
(sloreje	= 3.)	Lower K-sigma rejection limit in sky sigma
(shireje	= 3.)	Upper K-sigma rejection limit in sky sigma
(khist	= 3.)	Half width of histogram in sky sigma
(binsize	= 0.1)	Binsize of histogram in sky sigma
(smooth	= no)	Boxcar smooth the histogram
(rgrow	= 0.)	Region growing radius in scale units
(mksky	= no)	Mark sky annuli on the display
(mode	= ql)	
($nargs	= 0)	

PACKAGE	= apphot
TASK	= photpars

(weighti	= constant)	Photometric weighting scheme for wphot
(aperture	= (salgori=centroid)	Sky fitting algorithm) List of aperture radii in scale units
(zmag	= 25.)	Zero point of magnitude scale
(mkapert	= no)	Draw apertures on the display
(mode	= ql)	
($nargs	= 0)	

PACKAGE	=	apphot
TASK	=	polypars

(zmag	= 25.)	Zero point of magnitude scale
(mkpolyg	= no)	Draw polygon on the image display
(mode	= ql)	
($nargs	= 0)	

APPENDIX C

IRAF scripts written to automate the analysis

Group images by applied filter

```
#@allfiles is the list of all science frames
list="allfiles"
while(fscan(list,s1)!=EOF){
imgets((s1),"FILTA")
s2=(imgets.value)
print((s1),>>(s2)//".list")
print(s2)
```

```
}
```

Extraction of Julian Date from images

```
#B.list contain all B filter images
#Julian dates are recorded in the list JD_B.list
list="B.list"
while(fscan(list,s1)!=EOF){
imgets(s1,"JD")
s2=(imgets.value)
print(s2, >>"JD_B.list")
}
```

Grouped images into 50-image sets

```
#This script will make image sets of 50 images in folders
#Change the list name as wish,R.list process R filter images
#Directory paths and urls can be changed

list="R.list"
int filenum=0
while(fscan(list,s1)!=EOF){

#Change the destination folder of images, R for R filter images
imcopy((s1),("R"))
filenum+=1
}
print(filenum //" files were copied...")
cd("R")
files("*.fits",>>"R.list")

int numfolders=0
numfolders=(filenum/50)+1
print(numfolders // " folders to create...")

i=1
while(i<=numfolders)
{

mkdir("imset"//i)
print("creating folder imset"//i )

i+=1
}
```

```
int newi=1
list="R.list"
int filecount=0
while(fscan(list,s1)!=EOF)
{

if (filecount>=50)
{
newi+=1
filecount=0
}

imcopy((s1),("imset"//newi))
filecount+=1

}
imdelete("@R.list")

i=1

#copy nessery files into the folders
while(i<=numfolders)
{
cd("imset"//i)
files("*.fits",>>"imset.list")
mkdir("shifted")
cp("/home/danula/iraf/PH483/28Jun2015/scripts/displayimages.cl",".")
cp("/home/danula/iraf/PH483/28Jun2015/scripts/my scripts/Image shift/shiftimage.cl",".")

list="imset.list"
while(fscan(list,s1)!=EOF){
imgets(s1,"JD")
s2=(imgets.value)
print(s2, >>"JD.list")
}

cd("..")

i+=1
}

list="imset.list"
i=0
while(fscan(list,s1)!=EOF){

imshift(s1,"shifted/s"//s1,(-0.09*i),(-0.72*i))
i+=1
}
```

```
cd("shifted")
files("*.fits",>>"imset.list")
cp("/home/danula/iraf/PH483/28Jun2015/scripts/displayimages.cl",".")
cp("/home/danula/iraf/PH483/28Jun2015/scripts/coor1.coo",".")
```

Perform photometry using phot in the batch mode

```
#This script will process the phot in batch mode
# @urls and .mag file names can be changed
i=1
while(i<17){
cd("imset"//i)
cd("shifted")
phot(" *.fits"," coords=coor1.coo");
txdump("*.mag","ID,XCENTER,YCENTER,MAG,MERR,PERROR","yes",>"mag"//i//".dat")
cp("mag"//i//".dat","@url")
cd("..")
cd("..")
i+=1
}
```

Display images using DS9 image server.

```
cl>!ds9 &
```

```
list="imset.list"
while(fscan(list,s1)!=EOF){
display(s1)
}
```

APPENDIX D

VARTOOLS Commands

Applying LS method to the Lght curve

```
vartools -i LC_V _SZLyn -oneline \
   -LS 0.1 10. 0.1 5 1 /OUTDIR1 whiten clip 5. 1
```

Run the Lomb-Scargle period-finding algorithm on the light curve LC_V _SZLyn.Search for periods between 0.01 and 2.0 days at a frequency resolution of 0.01/T (T is the time-span of the Light Curve). Report the top 5 peaks, and output the periodogram to OUTDIR folder(the filename will beLC_V _SZLyn.ls). Pre-whiten the light curve and re-apply L-S before finding the next peak, and use a 5 sigma iterative clipping in determining the spectroscopic S/N.

```
Name                      = LC_V _SZLyn
LS_Period_1_0             =    0.11807771
```

Log10_LS_Prob_1_0   = -393.58637
LS_Periodogram_Value_1_0   =   0.81987
LS_SNR_1_0   = 29.29487
LS_Period_2_0   =   0.05847924
Log10_LS_Prob_2_0   = -129.57662
LS_Periodogram_Value_2_0   =   0.43404
LS_SNR_2_0   = 17.07566
LS_Period_3_0   =   0.03973952
Log10_LS_Prob_3_0   = -51.01921
LS_Periodogram_Value_3_0   =   0.20434
LS_SNR_3_0   =   8.36644

Applying discrete Fourier transformation

vartools -i LC_V _SZLyn -oneline -ascii \
   -dftclean 10 maxfreq 40. outdspec OUTDIR

Compute the Discrete Fourier Transform (DFT) of the light curve LC_V _SZLyn. We will over-sample the DFT by a factor of 10, and compute the DFT up to a maximum frequency of 40 cycles per day. The resulting power spectrum will be output to the directory OUTDIR with the filename LC_V _SZLyn.dspec. We search for the highest peak in the power spectrum using a 5-sigma iterative clipping to determine the spectroscopic signal-to-noise ratio of the peak.

Name   = LC_V _SZLyn
DFTCLEAN_DSPEC_PEAK_FREQ_0_0 =   8.53658537
DFTCLEAN_DSPEC_PEAK_POW_0_0 = 0.0112711
DFTCLEAN_DSPEC_PEAK_SNR_0_0 = 34.0864
DFTCLEAN_DSPEC_PEAK_FREQ_1_0 =   17.47967480
DFTCLEAN_DSPEC_PEAK_POW_1_0 = 0.0016871
DFTCLEAN_DSPEC_PEAK_SNR_1_0 = 4.68075
DFTCLEAN_DSPEC_PEAK_FREQ_2_0 =   23.17073171
DFTCLEAN_DSPEC_PEAK_POW_2_0 = 0.000520221
DFTCLEAN_DSPEC_PEAK_SNR_2_0 = 1.10054

Converting Light curves into amplitude vs. phase diagrams

vartools -i LC_V _SZLyn -header \
   -Phase fix 1.2354 \
   -o LC_V _SZLyn_phase.txt

Phase the light curve LC_V _SZLyn with a period 0.1181 days and output the result to LC_V _SZLyn_phase.txt